

Tom Richard Evensen

Nanoparticles in dilute solution:

A numerical study of rotational diffusion

Thesis for the degree philosophiae doctor

Trondheim, June 2008

Norwegian University of Science and Technology
Faculty of Natural Sciences and Technology
Department of Physics



NTNU

Norwegian University of Science and Technology

Thesis for the degree philosophiae doctor

Faculty of Natural Sciences and Technology
Department of Physics

© Tom Richard Evensen

ISBN 978-82-471-1103-1 (printed version)

ISBN 978-82-471-1104-8 (electronic version)

ISSN 1503-8181

Doctoral theses at NTNU, 2008:209

Printed by NTNU-trykk

Abstract

This thesis is dedicated to Brownian dynamics simulations of rotational diffusion. A rotation dynamics engine has been implemented and tested. This engine will in the future be integrated as a part of a complete Brownian dynamics simulation tool. The special case, when translational motion can be ignored, has thoroughly been studied.

Two choices of generalized coordinates describing angular orientation of the particles are used. The Euler angles, which constitute the classical choice, and the Cartesian components of the rotation vector, which was recently introduced as an alternative, are being compared with regards to computational efficiency. Results from both equilibrium and non-equilibrium simulations are presented. The consistency of two new algorithms is demonstrated on systems of free rigid particles with arbitrary surface topographies. The algorithms make use of only the principal values of the rotational mobility tensor, assuming the corresponding principal axes coincide with the body-fixed coordinate system. These three scalars contain all information about the particle surface topography relevant for rotational diffusion. The calculation of the mobility tensor can be performed in a pre-calculation step, which makes the algorithm itself highly efficient. Both choices of generalized coordinates correctly reproduce theoretical predictions, but we have found that the algorithm using the Cartesian components of the rotation vector as generalized coordinates outperform its counterpart using the Euler angles by up to a factor 1000 in extreme cases. The reason for this improvement is that the algorithm using the Cartesian components of the rotation vector is free of singularities.

Preface

This PhD thesis presents work that has been carried out over a four year period (2004-2008) at the Department of Physics at the Norwegian University of Science and Technology (NTNU). During the same period I have also been taking courses and assisting students in the electronics and instrumentation laboratories. This amounts to about 50-60% of the time spent at the Department of Physics.

My PhD research has been made possible because of financial support by the Norwegian Research Council (Grant 158541/431) and the Department of Physics.

Professor Arnljot Elgsaeter has been my supervisor. He has provided excellent guidance and support during the whole period. His enthusiasm and numerous amusing stories have been a source of great inspiration during times of uphill struggle. I would also like to express my gratitude to my co-advisor, Professor Arne Mikkelsen, for his accurate and to the point tutoring and discussions.

My parents have always taken great interest in my education and work. Without their encouragement, all this would not have been possible.

To Stine, my friend, my love, my everything: Your patience, love and support during these years has been a tremendous inspiration. You bring out the best in me. With all my heart I thank you!

Trondheim, June 2008

Tom Richard Evensen

List of papers

The papers included in this thesis represent the research that I have been involved in during my PhD studies. All papers are self-contained.

Paper I [1]

Transient molecular electro-optics. Cartesian rotation vector versus Eulerian angles.
T.R. Evensen, A. Elgsaeter, and S.N. Naess, Colloids and Surfaces B, **56**, 80-86 (2007).

Paper II [2]

Free Rotational Diffusion of Rigid Particles with Arbitrary Surface Topography: A Brownian Dynamics Study Using Eulerian Angles.
T.R. Evensen, S.N. Naess and A. Elgsaeter, Macromol. Theory Simul., **17**, 121 (2008).

Paper III [3]

Brownian Dynamics Simulations of Rotational Diffusion: Rotation Vector versus Euler Angles.
T.R. Evensen, S.N. Naess and A. Elgsaeter, Macromol. Theory Simul. (2008), *accepted*.

Paper IV [4]

Brownian Dynamics Simulations of Electro-Optics: Rotation Vector versus Euler Angles
T.R. Evensen, S.N. Naess and A. Elgsaeter, Macromol. Theory Simul. (2008), *submitted*.

Contents

1	Introduction	1
1.1	Brownian dynamics simulations	5
1.1.1	Background	5
1.1.2	Simulation techniques	7
1.1.3	Generalized coordinates	10
1.1.4	Fokker-Planck equations	13
1.1.5	Stochastic differential equations	14
1.1.6	Numerical algorithms	15
1.1.7	Micro Fluid Dynamics	16
1.1.8	Metric Force	21
1.2	Electro-optics	22
2	Concluding remarks and future perspective	27
3	Summary of papers	29
	References	31
A	Collection of papers	34

Chapter 1

Introduction

This chapter presents the background, on which the work of this thesis is based. In addition, a few of the key arguments and results are repeated.

This thesis focuses on Brownian dynamics simulation of rigid particles in dilute solution. The particles of main interest are biopolymers, which are molecules of biological origin. The length of these molecules are in the range 1 nm to 1 μm , and their weight are $10^3 - 10^7$ g/mol. Characteristic times for biopolymer dynamics are in the range ps to ns. Biopolymers can be divided into three main groups: A) Proteins or polypeptides, B) Polysaccharides, and C) Polynucleic acids (RNA/DNA). Figure (1.1) shows sketches of these types of biopolymers. In order to fully understand the functional roles of a biopolymer, it is often sufficient to study the atomic structure. In many cases, however, the dynamics of the particle plays an important role, and it is necessary to study the biopolymer further. For example, the rate of a process, which requires the docking of two particles, will strongly depend on the fraction of time the two particles have a particular angular orientation relative to each other.

My main interest was to establish an algorithm able to study the dynamics of such systems. Dynamics studies are important in order to understand quantitatively measurements of nanoparticle transport properties. Measurements based on thermally induced density and conformational fluctuations cannot be analyzed quantitatively without detailed modeling and analysis of the dynamics. Common are measurements of translational and rotational diffusion, sedimentation and electrophoresis.

Understanding polymer dynamics is important in industry and technology in connection with processing of food, plastic manufacture, movement of biological fluids, performance of lubricants, application of paint etc. During manufacturing and production, the polymers are in liquid state. The flow and transport properties of polymers differ from standard Newtonian flow behavior. Some examples of this unusual behavior are shear thinning, rod climbing, and viscoelasticity. This non-Newtonian flow behavior of polymer liquids must be considered. Dynamics studies of polymer systems are therefore an important and

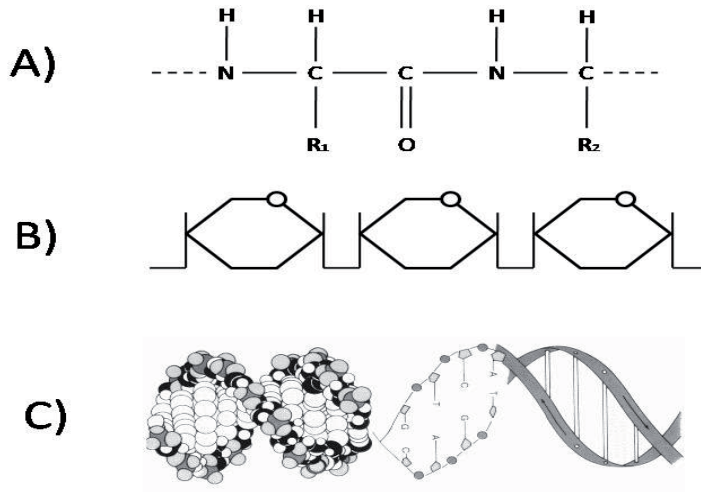


Figure 1.1: A schematic sketch of the three main groups of biopolymers. A) Proteins (polypeptides), B) Polysaccharides, and C) Polynucleic acids: double helix DNA ("The DNA Page" <http://members.lycos.nl/TheDNApage/index.html>)

rapidly growing branch of science.

The theory for describing the Brownian dynamics of polymer models consisting of spherical subunits is well established [5, 6]. For many years it was believed that the extension to non-spherical subunits would be too difficult and even impossible. The exponential growth in computer power over the last twenty years has made it possible to perform quantitative simulations of non-spherical nanoparticles in solution. For instance, the simulations in this thesis were carried out on standard PCs common in most homes today. Figure (1.2) provides a sketch of these two polymer models.

To put this thesis into context, a description of the research philosophy of our group is in order. Our main goal is to make the connection between nanoscopic and macroscopic properties of rigid particles with arbitrary surface topography in dilute solutions. Our primary aim is to make predictions of macroscopic properties using simulations, and deductions of nanoscopic properties from experimental result. The precision of these predictions and deductions should be at least one order of magnitude higher than the current standard. The following plan has been devised in order to achieve this goal:

1. Introduce a precise formal theory for the Brownian dynamics of particles with arbitrary shape or surface topography.
2. Develop Brownian dynamics algorithms able to perform quantitative simulations based on the formal theory described in step 1.

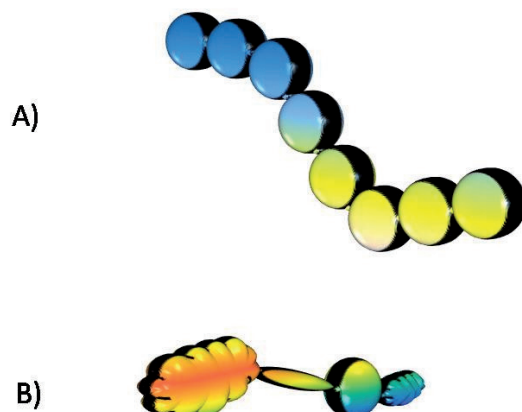


Figure 1.2: Schematic sketch of two types of polymer models. A) Model consisting of spherical subunits. B) Model consisting of non-spherical subunits.

3. Implement the sufficiently effective algorithms described in step 2.
4. Perform quantitative simulations of nanoparticles in solution based on the effective algorithms from step 3.
5. Establish state-of-the-art instruments for precise measurements of nanoparticles in solution.
6. Perform precise measurements of nanoparticles in solution using the state-of-the-art instruments from step 5.

The precise formal Brownian dynamics theory of step 1, and the development of the associated algorithms (step 2) were carried out mainly by Naess and Elgsaeter [7, 8, 9, 10], and the same authors have initiated work regarding the steps 5 and 6. The implementation of the algorithms (step 3) and the execution of quantitative simulations based on these implementations (step 4) are being partly addressed in the current thesis.

By performing computer simulations, one can expose nanoparticle systems to virtually every imaginable condition; conditions that are impossible to realize experimentally. At this point, it is important to remember that, although an important scientific tool, computer simulations only produce results that are as good, or as bad, as the theory on which they are based. Computer simulations could therefore never replace real experiments, which provide true information about the physical system. As such, the experimental steps 5 and 6 are crucial for identifying mistakes in both theory and algorithms. When all the steps listed above are completed, our intention is to compare simulation results obtained

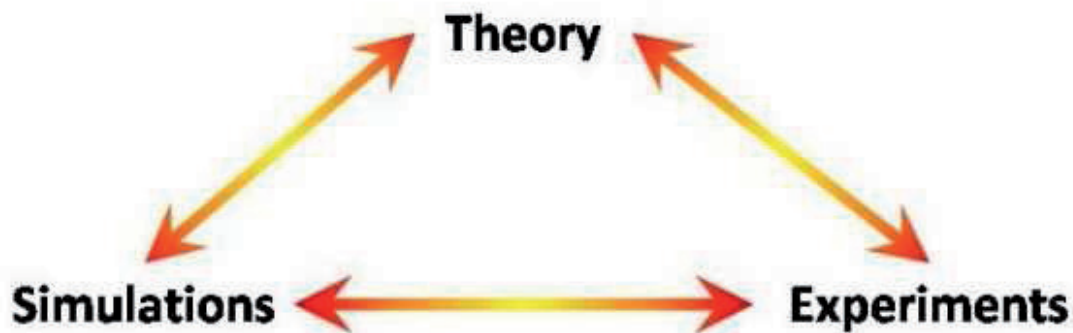


Figure 1.3: Integration of theory, simulations, and experiments is important to reach our declared goal.

in step 4 and experimental data obtained in step 6. By integrating theory, simulations, and experiments, as shown in Fig. 1.3, we believe that new information and details about nanoparticle systems are revealed, and that these revelations would be of significant value for future nanoparticle research and technology.

My thesis is an important part of a project where the primary objective is to develop an efficient general algorithm for Brownian dynamics simulations of polymers consisting of arbitrarily shaped rigid particles either free or linked in chains. The goal of this ongoing project is to include translational-rotational fluid dynamic coupling for each individual segment, full fluid dynamic interaction between all pairs of segments, freely selectable linkage points on the particle surfaces, spring potential links, and holonomic constraints. To ensure that the Brownian dynamics algorithm yields equilibrium results in agreement with the generalized Boltzmann equilibrium probability densities, generalized coordinates are used to describe particle translation and angular orientation. This also ensures that the algorithm at all times yields results consistent with the fluctuation dissipation theorem.

We have chosen the Cartesian components of the rotation vector as generalized coordinates describing angular orientation. Theoretical studies [9, 10] suggest that this choice should yield algorithms free of singularities observed when using the Euler angles as generalized coordinates. The focus of my thesis has been to develop and test the rotational dynamics engine of the new Brownian dynamics algorithm. These tests have been devised in order to compare the two choices of generalized coordinates. In order to study the characteristics of the rotational dynamics engine, we have developed an analytical expression for the 3×3 rotational mobility tensor for the special case when translational motion can be ignored. Our results indicate that this is a highly efficient method. The systems I have studied consists of free rigid particles of arbitrarily surface topography.

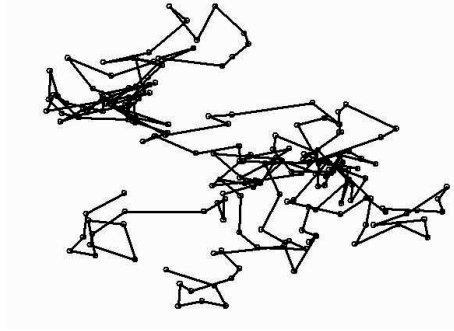


Figure 1.4: An illustration of the position of a Brownian particle as a function of time.

1.1 Brownian dynamics simulations

1.1.1 Background

The phenomenon known today as Brownian motion was first discovered by the Dutch scientist Jan Ingen-Housz in 1784 [11]. However, it was later named after the Scottish botanist Robert Brown, who in 1827, several years after Ingen-Housz had passed away, published his work on the subject [12]. Brown studied the erratic and random motion of small particles originating from pollen grains in water. His initial conclusion was that the particles moved because the pollen grains were alive, but he later found that particles from dead pollen grains as well as particles from other materials, such as minerals, also exhibited the same characteristic motion. Experiments conducted by Brown and others also showed that the motion depended on particle size, temperature and fluid viscosity. While earlier explanations of the behavior included evaporation, electric forces, and interaction with light, the true reason behind this phenomenon was not understood until several years later. As it turned out, the discovery of Brownian motion became one of the first evidences of the existence of molecules.

During the late 19th century, the development of kinetic theory of matter brought about the first qualitative explanation for the motion studied by Brown. The fluid molecules are in constant thermal motion. The velocity distribution of these molecules, the Maxwell distribution, depends on the temperature. Suspended particles collide with the solute molecules, and because of these impacts the particles move. The Brownian motion is the resultant effect of these collisions. Fig. (1.4) gives an illustration of a two-dimensional trajectory of a Brownian particle as a function of time. Famous publications on the topic of Brownian motion include those of Albert Einstein [13] and Paul Langevin [14]. An

English translation of the latter work is available in [15].

The paper by Langevin presents the first equation describing Brownian motion. The driving force on the Brownian particle is modeled as random noise containing the full range of frequency components. Because only the statistical properties of this force are known, this class of equations is commonly referred to as stochastic differential equations, and there are similar limitations on what can be predicted about the position coordinates of the Brownian particles. The Langevin equation yields invaluable insight into the relation between thermal molecular motions and simple macroscopic diffusion.

Despite its huge success, the Langevin equation appears to be the result of mainly well educated guessing. It was not until 1969 that Zwanzig [16] for certain systems derived the rigorous equivalence between the generalized diffusion equations and stochastic differential equations describing Brownian motion. He also pointed out the fundamental importance of this finding with regard to how new Brownian dynamics algorithms should be established. The procedure initiated by Zwanzig consists of three steps:

- I) Development of the generalized diffusion equation (Fokker-Planck equation) for the molecular model of interest.
- II) Establish a stochastic differential equation which yields the same statistical characteristics as the generalized diffusion equation established in step I.
- III) Development of a numerical algorithm that yields trajectories with statistical characteristics in agreement with stochastic differential equation established in step II.

This constitutes the Golden Rules of Brownian Dynamics. The theoretical foundation of step III was published in 1978 by Fixman [17, 18]. In the same year Ermak and McCammon published another influential work on parts of the same topic [19].

A superb account of all three steps of this process can be found in the monograph published in 1996 by Öttinger [6]. A highly regarded presentation of the complementary kinetic theory is available in the book by Bird et. al. [5].

Combining multiple particles into chains has also been an important field of research. Kramers [20] investigated the statistical behavior of polymer chains using kinetic theory on beads interconnected by rods. This specific type of polymer chain model has consequently been named Kramers chains. Rouse [21] and Zimm [22] introduced the bead-spring model, where the beads are interconnected with spring potentials. For pure Hookean springs, the bead-spring chain is usually referred to as a Rouse chain. A Kramers chain and a Rouse chain are shown in Figure (1.5). The first to use kinetic theory in order to derive a Fokker-Planck equation for polymers in solution was Kirkwood [23]. Because the Hookean spring potential in principal allows the chain to extend infinitely, several amendments have been introduced. The most successful in this regard is maybe the FENE model [24], which uses a non-linear spring force with limited extensibility.

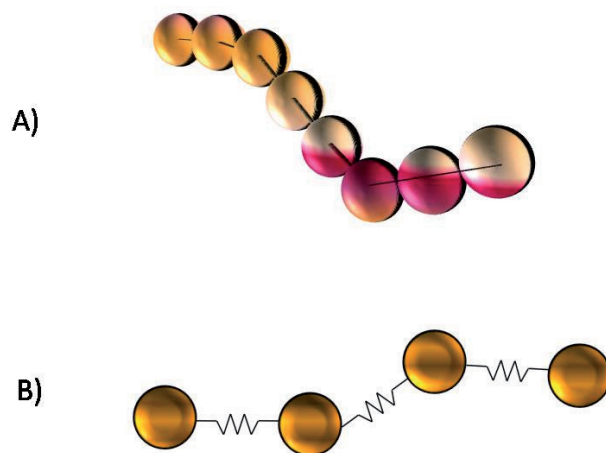


Figure 1.5: Polymer chain models. A) Kramers chain consisting of spherical beads interconnected by rods. B) Rouse chain consisting of spherical beads interconnected by Hookean springs.

Rotational Brownian diffusion of large biomolecules has long been a favored topic in biophysics. Some of the earliest analytical studies of molecular rotational Brownian motion were published in 1929 by Debye [25]. Shortly thereafter Perrin solved the rotational diffusion equation for prolate ellipsoids [26]. In 1960 a full analytical analysis of the rotational Brownian motion of free rigid bodies with arbitrary shape was carried out by Favro [27]. The theory of anisotropic rotational diffusion has since been applied to the analyses of the data from a long list of experiments. These include measurements of transient electric birefringence and dichroism, dielectric relaxation, electron spin resonance line widths, NMR quadrupolar relaxation, fluorescence depolarization and dynamics light scattering.

1.1.2 Simulation techniques

Although the kinetic theory of polymers in solution is well understood, the theory quickly gets too complicated to be solved analytically. Analytical expressions can be found only for the simplest cases. In order to obtain results for more complex models and conditions, numerical simulations must be employed. The most common simulation techniques are Monte Carlo simulations, molecular dynamics simulations, and Brownian dynamics simulations [28].

Monte Carlo simulations are useful when studying equilibrium properties of particles in solution. These particles can be free rigid nanoparticles, or long, interconnected polymer chains. The technique relies on statistical mechanics and generates new states according

to appropriate Boltzmann distributions. The macroscopic properties are then computed as an average over an ensemble of particle conformations. However, Monte Carlo simulations are less suited for studying non-equilibrium properties because the non-equilibrium probability distribution, from which new states are sampled, is rarely known a priori. Also, the time t is not a parameter in this technique.

The second commonly employed technique, molecular dynamics (MD) simulations, describes the entire system, nanoparticles and solvent particles, at an atomic scale. All the atoms behave as if in vacuum, except for interactions with neighboring atoms and external forces. The deterministic dynamics of the atoms are calculated using classical mechanics, i.e. Newton's laws of motion, once the atom coordinates in phase space, atom masses, and interaction potentials are known. When all this information is available at time $t = 0$, the state of the entire system can in principle be determined for any time t in the future. The time scale of the MD-technique is, however, usually limited to one nanosecond because of the small time steps required to handle the rapid movement of the solvent molecules. The large number of variables needed to describe the entire system, and the small time steps, renders this technique useless for a full MD-simulation of polymers or rigid particles in solution. A second issue is that after a relatively small number of collisions, a stochastic element is introduced because of phase space dependent velocity changes resulting from various types of collisions. The accuracy of computer number representation is not high enough to deal with these changes. Consequently, the deterministic process still becomes stochastic.

In Brownian dynamics (BD) simulations, the solvent is modeled as a continuum which influences the polymers through both a deterministic frictional force and a stochastic Brownian force. This approach has been used in polymer physics since the late 1970s, and has been proven as the only feasible alternative for simulations of polymers in solution.

One of the most cited papers on Brownian dynamics is Ermak and McCammon [19]. These authors carried out simulations for bead-spring chains with fluid dynamic interaction. Allison and McCammon [29] introduced a similar algorithm using bead-rod chains. This algorithm proved to yield erroneous results, and Öttinger [30] published an alternative and correct algorithm. Antosiewicz, Grycuk and Porschke [31] based their algorithm on the work of Ermak and McCammon, but used the rotation vector to represent the angular orientation of rigid particles. Brownian dynamics algorithms where the polymer chains are modeled using non-spherical subunits have been addressed by several authors. One attempt by Garcia de la Torre [32] involves modeling the non-spherical subunits using a large number of densely packed beads. This approach has the major drawback that all beads must be incorporated in the BD-simulations. This has the unfortunate effect of introducing degrees of freedom that have no physical significance. Most of the simulation time is spent calculating internal dynamics related to these degrees of freedom. In addition, the stiffness of the interconnecting springs must be very high, resulting in very small time steps. Because of this, only the simplest cases can be studied with success using this approach.

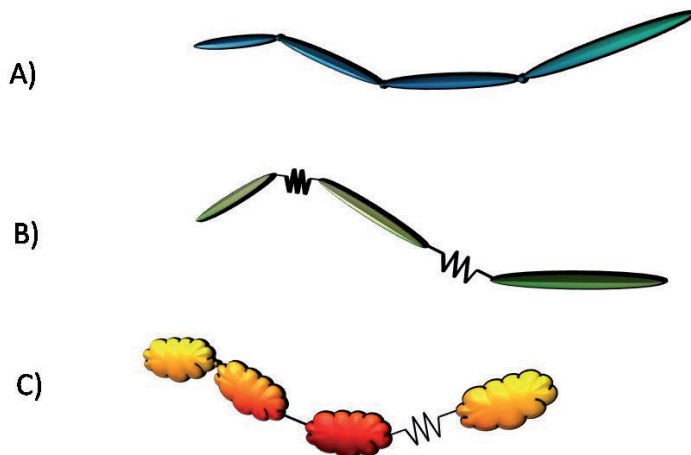


Figure 1.6: Schematic sketches of A) needle chain, B) needle spring chain, and C) chain of arbitrarily shaped subunits interconnected with ball socket joints, rigid rods and springs.

In order to avoid this problem, Nyland et al. [33] introduced the first BD-algorithm for needle chains, which contains only the degrees of freedom relevant for the problem. The superior efficiency of this algorithm relative to the Ermak-McCammon algorithm was demonstrated by Skjetne and Elgsaeter [34]. The first algorithm for BD-simulations using needle spring chains was introduced by Mikkelsen et al. [35], and the authors Klavness and Elgsaeter [36] derived the first algorithm for Brownian dynamics simulations of polymers consisting of subunits with arbitrary shape interconnected by rigid rod, ball socket joints or springs. This algorithm is rigorously derived from kinetic theory, and the aspect of translational-rotational fluid dynamic interactions in BD-simulations of non-spherical subunits was first introduced in this paper. Naess and Elgsaeter [8] corrected this algorithm by including the component $\vec{\mathcal{F}}^{(m,g)}$ of the metric force. These authors also developed the algorithm further by changing the generalized coordinates describing angular orientation [7, 9, 10]. Substituting the commonly used Euler angles with the Cartesian components of the rotation vector they arrived at an algorithm free of singularities. Figure (1.6) shows schematic sketches of needle chain, needle spring chain, and a chain of arbitrarily shaped subunits interconnected with ball socket joints, rigid rods and springs.

The most popular Brownian dynamics algorithm for rotational diffusion can be traced back more than two decades [37, 38, 39]. This algorithm is not derived from kinetic theory. It does not include a set of generalized coordinates, but keeps track of the body-fixed coordinate system in laboratory coordinates. Consequently, this algorithm does not follow the Golden Rules of Brownian dynamics described in the previous section. The formulation of Brownian dynamics algorithms based on the generalized Langevin equations is notoriously difficult and commonly leads to mistakes. Another such example is the once highly regarded SHAKE-HI algorithm [29]. In all work done prior to 2003 the

popular BD-algorithm contained an error in the way the Brownian increment was added. After more than 20 years of use, this error was finally recognized and corrected by the introduction of the so-called unbiased rotational move [40].

1.1.3 Generalized coordinates

From classical mechanics, it is known that a rigid particle with no axial symmetries has six degrees of freedom [41]. This means that at least six coordinates are required in order to fully describe position and angular orientation of the particle. If the number of coordinates is identical to the number of degrees of freedom, the coordinates are known as generalized coordinates. To specify the position and orientation of a rigid body, three Cartesian coordinate systems are needed as shown in Figure (1.7):

- Laboratory coordinate system with axes (x, y, z) .
- Local coordinate system with origin fixed in the particle and with axes, $(x^{(l)}, z^{(l)}, z^{(l)})$, parallel with the laboratory axes.
- Body-fixed coordinate system with both origin and axes, $(x^{(\text{bf})}, z^{(\text{bf})}, z^{(\text{bf})})$, fixed in the particle.

The origin of the local and the body-fixed coordinate systems are usually placed in the particle mass or hydrodynamic center. The position of the origin of the local coordinate system relative to the laboratory coordinate system is given by the position vector \vec{r}_c . This gives the position of the particle, while the orientation of the particle is given by the orientation of the body-fixed coordinate system relative to the local coordinate system. The classical choice of generalized coordinates describing particle angular orientation in Brownian dynamics algorithms are the Euler angles, (ϕ, θ, ψ) , as shown in Figure (1.7). In this thesis, y -convention Euler angles has been used. The first rotation, ϕ , is about the body-fixed $z^{(\text{bf})}$ -axis. The second rotation, θ , is about the new $y^{(\text{bf})}$ -axis, and the last rotation, ψ , is about the resulting new $z^{(\text{bf})}$ -axis. The term y -convention refers to the second rotation, which is about the new orientation of the body-fixed $y^{(\text{bf})}$ -axis. In the x -convention Euler angles, the second rotation is about the body-fixed $x^{(\text{bf})}$ -axis. Note that in y -convention Euler angles, the first two rotations, ϕ and θ , are identical to the polar angles. In chapter 1.1.6, we will demonstrate that using the Euler angles in Brownian dynamics simulations yields algorithms that contain severe singularities.

The Cartesian components of the rotation vector were recently introduced as an alternative in Brownian dynamics algorithms by Naess and Elgsaeter [9]. Figure (1.8) gives an illustration of this option. The Euler theorem [41] states that, angular orientation resulting from an arbitrary sequence of individual rotations of a rigid body always can be obtained by one single rotation of the rigid body about a given axis. For a given final orientation of the rigid body, both the angle of rotation Φ and the unit vector of the

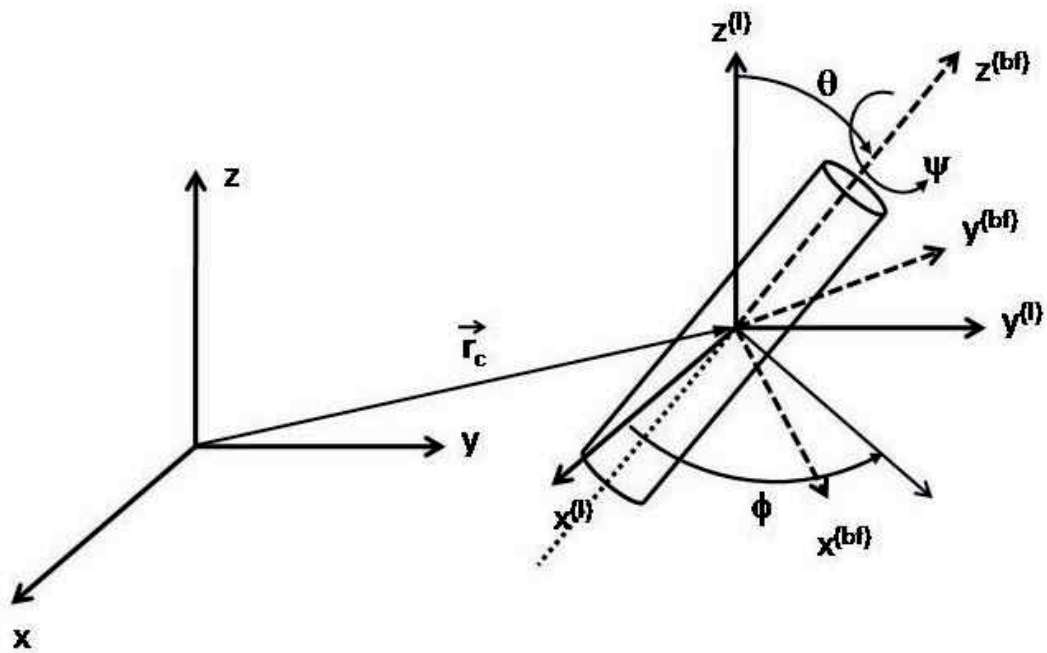


Figure 1.7: To fully describe the position and orientation of a particle we need three Cartesian coordinate systems. The position of the origin of the local coordinate system is given relative to the laboratory coordinate system by the position vector \vec{r}_c . The orientation of the body-fixed coordinate system relative to the local coordinate system is given by three coordinates, in this case the Euler angles (ϕ, θ, ψ) . The orientation of the body-fixed axes after the last rotation, ψ , is not shown in this illustration.

rotation $\vec{\delta}^{(a)}$ are unique. Each angular orientation corresponds to one point in the coordinate space, and vice-versa. The rotation vector describing the new angular orientation is defined as $\vec{a} := \Phi \vec{\delta}^{(a)}$. In the literature, alternative definitions have also been adopted in otherwise unrelated fields of science [42]. This reference introduce a vector parameterization of rotation $(g, \vec{\delta}^{(a)})$, where $g = g(\Phi)$ is the generating function, and $\vec{a} := g(\Phi) \vec{\delta}^{(a)}$. In this thesis, we have studied the generating function $g(\Phi) = \Phi$.

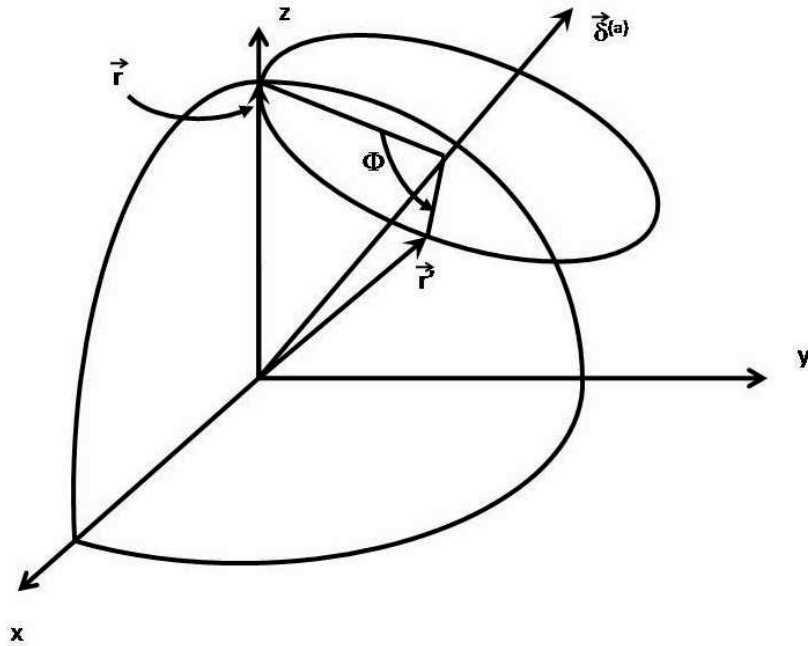


Figure 1.8: Illustration of the Cartesian rotation vector. The Cartesian components of the rotation vector constitute an alternative to the Euler angles describing particle angular orientation, and are given by $\vec{a} = \{a_1, a_2, a_3\} := \Phi \vec{\delta}^{(a)}$, where Φ is the angle of rotation about the unit vector $\vec{\delta}^{(a)}$. The reference orientation of the body-fixed position vector, \vec{r} , is along the z-axis of the laboratory coordinate system. After a rotation Φ about $\vec{\delta}^{(a)}$, the body-fixed position vector is changed to \vec{r}' .

The coordinate space of the rotation vector can be subdivided into infinitely many concentric spherical shells around a spherical subspace with its center at the origin of the fixed Cartesian laboratory coordinate system. The radius of the spherical subspace equals 2π and the concentric spherical shells all have thickness 2π . Each of these subspaces contain identical information about the particle angular orientation (Φ and $\Phi + 2\pi$ constitute the same physical orientation). Brownian dynamics simulations can therefore be limited to any of these subspaces, but for each of these subspaces the numerical algorithms show weak singularities at the subspace boundaries. The coordinate space can be limited even further. It can be derived, because of symmetry reasons, that the inner half of the spherical subspace described above, i.e. for $a < \pi$, contains all possible particle orientation. In

chapter 1.1.7, we see that, in this subspace, the BD-algorithm displays no singularities [10].

The work and papers presented in this thesis contain simulation results based on algorithms using these two choices of generalized coordinates describing angular orientation.

1.1.4 Fokker-Planck equations

The Fokker-Planck equation (diffusion equation) is mathematically a linear second-order partial differential equation of parabolic type. This equation describes the time evolution of the probability density in coordinate space, $p(\vec{q}, t)$, where \vec{q} denotes particle position and parameter t is time. The equation is also known as the Smoluchowski equation or Kolmogorov's forward equation [43]. The Fokker-Planck equation is not restricted to systems near equilibrium, but may also be applied to systems in a non-equilibrium state. This equation has the general form [6]

$$\frac{\partial}{\partial t} p(\vec{q}, t) = - \sum_s \frac{\partial}{\partial q_s} [A_s(\vec{q}, t) p(\vec{q}, t)] + \sum_{tu} \frac{\partial^2}{\partial q_t \partial q_u} [D_{tu}(\vec{q}, t) p(\vec{q}, t)], \quad (1.1-1)$$

where \vec{A} denotes the drift vector and \vec{D} gives the diffusion properties. The first and second term on the right hand side is called the drift and diffusion term, respectively. Thus, the Fokker-Planck equation describes a combined drift and diffusion process with a continuous time parameter.

For systems with no fluid velocity field, it can be shown, using kinetic and stochastic theory as well as standard methods from statistical physics, that the general Fokker-Planck equation for the Brownian motion of rigid molecules reads [6, 8]

$$\begin{aligned} \frac{\partial}{\partial t} p(\vec{q}, t) = & - \sum_{i=1}^d \frac{\partial}{\partial q_i} \left\{ \sum_{j=1}^d \mu_{ij} [\mathcal{F}_j^{(\Phi)} + \mathcal{F}_j^{(e)} + \mathcal{F}_j^{(m,q)}] p(\vec{q}, t) \right\} \\ & - k_B T \sum_{i=1}^d \frac{\partial}{\partial q_i} \left\{ \left[\sum_{j=1}^d \frac{\partial}{\partial q_j} \mu_{ij} \right] p(\vec{q}, t) \right\} \\ & + k_B T \sum_{i,j=1}^d \frac{\partial}{\partial q_i} \frac{\partial}{\partial q_j} \{ \mu_{ij} p(\vec{q}, t) \}. \end{aligned} \quad (1.1-2)$$

Here, d is the number of degrees of freedom, k_B is the Boltzmann constant, and T is the absolute temperature. The parameters μ_{st} are the components of the particle mobility tensor $\vec{\mu}$. The vector $\vec{\mathcal{F}}^{(\Phi)}$ is the conservative spatial force derived from intra molecule potentials, i.e. excluded volume forces. The force $\vec{\mathcal{F}}^{(e)}$ is the generalized deterministic force associated with external potentials, such as electric potentials or particle buoyancy. The generalized metric force $\vec{\mathcal{F}}^{(m,q)}$ ensures that for any choice of generalized coordinates

and for any positive semi-definite mobility tensor, the equilibrium probability density equals the Boltzmann distribution.

Except for the simplest system conditions, the Fokker-Planck equation cannot be solved analytically. When the number of degrees of freedom is large, parabolic partial differential equations are often impossible to solve using numerical methods. This poses an additional difficulty. For most particle systems the only viable option is therefore to solve the equivalent stochastic differential equation, which is the topic of the next section.

1.1.5 Stochastic differential equations

In physics literature, stochastic differential equations are commonly referred to as Langevin equations, after the French physicist Paul Langevin. The Langevin equation describes Brownian motion by using Newton's equation of motion. In this naive approach to stochastic differential equations, it is assumed that the total force on the particle is the sum of a frictional force and a random Brownian force. In one dimension we obtain [14, 15]

$$m \frac{dv}{dt} = -\zeta v + F^B, \quad (1.1-3)$$

where m is the particle mass, and v denotes the time-dependent particle velocity. The frictional force is proportional to and opposing the motion, and ζ is the frictional coefficient. The Brownian force is modeled by a stochastic process F^B , and is a consequence of the frequent impacts of fluid particles on the Brownian particle.

History has shown that "ad hoc" Langevin equations frequently lead to erroneous results. It is crucial that stochastic differential equations are rigorously derived. In our approach, the Fokker-Planck equation (1.1-2) is rigorously derived from kinetic theory and in this section we give the equivalent stochastic differential equation derived from this.

Öttinger [6] states the form of the general stochastic differential equation (SDE) as

$$\frac{d}{dt} \vec{q}(t) = \vec{A}(\vec{q}, t) + \sqrt{2} \vec{B}(\vec{q}, t) \cdot \vec{f}(t), \quad (1.1-4)$$

where the vector \vec{A} and matrix \vec{B} are arbitrary, and $\vec{f}(t)$ is a stochastic process. Our algorithm is based on stochastic processes where the integral of $\vec{f}(t)$ equals the Wiener process

$$d\vec{W}(t) := \int_t^{t+dt} \vec{f}(t') dt'. \quad (1.1-5)$$

The Wiener process can be realized in several ways. We use a Gaussian process with zero mean and standard deviation Δt . This way the standard deviation equals the time step in the numerical algorithm. Because of the large, and fundamental, difference between deterministic calculus and stochastic calculus, integration of Equation (1.1-4) using Riemann-integration produces erroneous results. Instead, Ito integration of Equation

(1.1-4) yields

$$d\vec{q}(t) = \vec{A}(\vec{q}, t) dt + \sqrt{2} \vec{B}(\vec{q}, t) \cdot d\vec{W}. \quad (1.1-6)$$

In general, Equation (1.1-6) gives a microscopic description of stochastic processes that, on the macroscopic level, consists of both drift and diffusion. The drift and diffusion processes are given as

$$\langle \vec{q}(t+dt) - \vec{q}(t) \rangle = \vec{A}(\vec{q}, t) dt \quad (1.1-7)$$

$$\langle (\vec{q}(t+dt) - \vec{q}(t))(\vec{q}(t+dt) - \vec{q}(t)) \rangle = 2 \vec{B}(\vec{q}, t) \cdot \vec{B}(\vec{q}, t)^T dt. \quad (1.1-8)$$

When the drift and diffusion processes described in the Fokker-Planck equation (1.1-2) and the stochastic differential equation (1.1-6) are identical, the two equations offer alternative descriptions of the same physical system. This will be satisfied when the drift vector is the same in both cases, and

$$\vec{D}(\vec{q}, t) = \vec{B}(\vec{q}, t) \cdot \vec{B}(\vec{q}, t)^T. \quad (1.1-9)$$

But, even when a decomposition $\vec{D} = \vec{B} \cdot \vec{B}^T$ is specified, there is not a one-to-one correspondence between the Fokker-Planck equation and the stochastic differential equation. The Fokker-Planck equation only specifies the distribution of the stochastic process, and the stochastic differential equation determines the actual trajectory. If \vec{B} satisfies (1.1-9) so does $\vec{B} \cdot \vec{S}$ if $\vec{S} \cdot \vec{S}^T = \vec{\delta}$, where $\vec{\delta}$ is the unity tensor. In other words, processes described by the stochastic differential equation can be different on the microscale, but still have identical Fokker-Planck equations. This is referred to as weak equivalence.

For rigid molecules, the Itô stochastic differential equation

$$\begin{aligned} dq_i &= \sum_{j=1}^d \mu_{ij} [\mathcal{F}_j^{(\Phi)} + \mathcal{F}_j^{(e)} + \mathcal{F}_j^{(m,q)}] dt \\ &+ k_B T \sum_{j=1}^d \frac{\partial}{\partial q_j} \mu_{ij} dt + \sqrt{2k_B T} \sum_{j=1}^d B_{ij} dW_j \end{aligned} \quad (1.1-10)$$

is weakly equivalent with the Fokker-Planck equation (1.1-2). Both Equation (1.1-9) and Equation (1.1-10) are valid for any choice of generalized coordinates. It is important to mention that the stochastic part of the dynamics is expressed in terms of the mobility tensor for deterministic motion. This is in accordance with the fluctuation-dissipation theorem [44].

1.1.6 Numerical algorithms

The Itô stochastic differential equation for rigid particles with arbitrary surface topography can readily be integrated using the standard Euler-Maruyama integration scheme [6].

The resulting numerical algorithm reads

$$\begin{aligned}
q_i(t + \Delta t) &= q_i(t) + \sum_{j=1}^d \mu_{ij} \left[\mathcal{F}_j^{(\Phi)} + \mathcal{F}_j^{(e)} + \mathcal{F}_j^{(m,q)} \right] \Delta t \\
&+ k_B T \sum_{j=1}^d \frac{\partial}{\partial q_j} \mu_{ij} \Delta t + \sqrt{2k_B T} \sum_{j=1}^d B_{ij} \Delta W_j,
\end{aligned} \tag{1.1-11}$$

or equivalently on vector form

$$\begin{aligned}
\vec{q}(t + \Delta t) &= \vec{q}(t) + \left[\vec{\mu} \cdot \left(\vec{\mathcal{F}}^{(\Phi)} + \vec{\mathcal{F}}^{(e)} + \vec{\mathcal{F}}^{(m,q)} \right) \right]_0 \Delta t \\
&+ k_B T \left[\frac{\partial}{\partial \vec{q}} \vec{\mu} \right]_0 \Delta t + \sqrt{2k_B T} \vec{B}_0 \Delta \vec{W},
\end{aligned} \tag{1.1-12}$$

The subscript $_0$, denotes that this value is obtained at time t . The matrix $\vec{B}^{\Rightarrow(n)}$ is usually obtained using Cholesky decomposition of $\vec{\mu}$, but we will demonstrate that there are other more computationally efficient methods.

The algorithm in Equation (1.1-12) constitutes the natural basis for Brownian dynamics simulations of systems containing rigid particles provided that the quantitative numerical values of the mobility tensor are available.

1.1.7 Micro Fluid Dynamics

My main focus in this thesis has been rotational diffusion, and comparing the computational efficiency of the corresponding algorithms when the Euler angles and the Cartesian components of the rotation vector are used as generalized coordinates. For such tasks, it is important to avoid unintentional skewing of the playing field in favor of one or the other algorithm. In our case, the challenge has been to find a procedure for calculating the rotational mobility tensor that does not favor the rotation vector over the Euler angles, and vice versa. In this section, we start by giving the theoretical background for the mobility tensor, followed by how this non-skewed playing field is obtained.

The Navier-Stokes equation for incompressible fluids reads

$$\rho \frac{D}{Dt} \vec{v}^{(\kappa)} = -\nabla p + \eta \nabla^2 \vec{v}^{(\kappa)} + \rho \vec{g}, \tag{1.1-13}$$

where ρ is the fluid mass density, $\vec{v}^{(\kappa)}$ is the fluid flow field, D/Dt denotes the substantial derivative $D/Dt = \delta/\delta t + \vec{v}^{(\kappa)} \cdot \nabla$. Parameter p is the fluid-dynamic pressure, η is the fluid viscosity, and \vec{g} denotes the gravitational field.

The Navier-Stokes equation is non-linear, because the term on the left hand side in the equation above is of order two in $\vec{v}^{(\kappa)}$. For steady laminar flow ($\frac{\partial}{\partial t} = 0$) and no fluid

inertia effects ($\rho_m \vec{v}^{(\kappa)} \cdot \nabla \vec{v}^{(\kappa)} = 0$), the Navier-Stokes equation becomes linear

$$-\nabla p + \eta_s \nabla^2 \vec{v}^{(\kappa)} = -\rho \vec{g}. \quad (1.1-14)$$

This is commonly referred to as creep flow or Stokes flow. A parameter called the Reynolds number is used to decide if the flow is laminar or turbulent. The Reynolds number is defined as

$$Re := \frac{\rho}{\eta} V_0 l_0, \quad (1.1-15)$$

where V_0 is a typical fluid velocity, and l_0 is a relevant length of the problem. For $Re \leq 0.1$ Eq. (1.1-14) provides a good description of the fluid.

From Eq. (1.1-14) we get the relation between the particle spatial velocity $\dot{\vec{r}}$ and the fluid-dynamic force $\vec{F}^{(\text{fd})}$ [45]

$$\vec{F}^{(\text{fd})} = -\vec{\zeta} \cdot (\dot{\vec{r}} - \vec{v}^{(\kappa)}). \quad (1.1-16)$$

In the general case the friction tensor, $\vec{\zeta}$ does not exist in a simple form, but for a single spherical nanoparticle we get

$$\vec{\zeta} = \begin{pmatrix} \zeta^{(t)} \vec{\delta} & \vec{\mathbf{0}} \\ \vec{\mathbf{0}} & \zeta^{(r)} \vec{\delta} \end{pmatrix} \quad (1.1-17)$$

and

$$\zeta^{(t)} = 6\pi\eta_s\sigma_\nu \quad (1.1-18)$$

$$\zeta^{(r)} = 8\pi\eta_s\sigma_\nu^3, \quad (1.1-19)$$

where $\zeta^{(t)}$ is the translational friction coefficient, $\zeta^{(r)}$ is the rotational friction coefficient and σ is the radius of the spherical particle. The relation between the friction tensor and the mobility tensor for a single rigid particle is given by

$$\vec{\zeta} := \vec{\mu}^{-1}. \quad (1.1-20)$$

Using Eq. (1.1-20) we rewrite Eq. (1.1-16)

$$\dot{\vec{r}} - \vec{v}^{(\kappa)} = -\vec{\mu} \cdot \vec{F}^{(\text{fd})}. \quad (1.1-21)$$

When only deterministic dynamics is studied and inertia forces can be neglected, the force balance of the particle reads [5]

$$\vec{F}^{(\text{fd})} + \vec{F}^{(\Phi)} + \vec{F}^{(e)} = \vec{\mathbf{0}}, \quad (1.1-22)$$

where $\vec{F}^{(\Phi)}$ is the conservative force derived from inter-particle potentials, i.e. excluded volume forces and $\vec{F}^{(e)}$ is the conservative force due to external potentials, such as particle

buoyancy. The particle surface topography affects the particle dynamics partly through the mobility tensor and partly through the excluded volume interactions.

As explained, the main focus of this thesis is rotational diffusion. Calculating the rotational mobility tensor in a manner which does not favor one algorithm over the other is the essential task when the relative efficiency of the two algorithms is to be compared. This is achieved by using the 3×3 rotational mobility tensor, $\overset{\Rightarrow}{\boldsymbol{\mu}}^{(\omega)}$, as the starting point for the calculation. Tensor $\overset{\Rightarrow}{\boldsymbol{\mu}}^{(\omega)}$ gives the relation between torque, $\vec{\boldsymbol{T}}$, and angular velocity, $\vec{\boldsymbol{\omega}}$. For any choice of generalized coordinates, $\vec{\boldsymbol{q}}$, describing angular orientation, there is a one to one relation between $\vec{\boldsymbol{\omega}}$ and generalized velocity $\dot{\vec{\boldsymbol{q}}}$ given by

$$\dot{\vec{\boldsymbol{q}}} = \overset{\Rightarrow}{\boldsymbol{\Xi}}^{(q)} \cdot \vec{\boldsymbol{\omega}}, \quad (1.1-23)$$

where $\overset{\Rightarrow}{\boldsymbol{\Xi}}^{(q)}$ is the transformation matrix. This gives the following expression for the rotational mobility tensor, which is equally simple for any choice of generalized coordinates [7, 2]

$$\overset{\Rightarrow}{\boldsymbol{\mu}}^{(q)} = \overset{\Rightarrow}{\boldsymbol{\Xi}}^{(q)} \cdot \overset{\Rightarrow}{\boldsymbol{\mu}}^{(\omega)} \cdot \overset{\Rightarrow}{\boldsymbol{\Xi}}^{(q)T}. \quad (1.1-24)$$

For particles with arbitrary surface topography the rate of energy dissipation associated with angular velocity, $\vec{\boldsymbol{\omega}}$, is given as

$$\bar{W} = \vec{\boldsymbol{T}}^T \cdot \vec{\boldsymbol{\omega}} = \vec{\boldsymbol{T}}^T \cdot \overset{\Rightarrow}{\boldsymbol{\mu}}^{(\omega)} \cdot \vec{\boldsymbol{T}}. \quad (1.1-25)$$

For all non-zero external torque, the rate of energy dissipation in a viscous medium is always non-negative, i.e. $\bar{W} \geq 0$. This means that the mobility tensor, $\overset{\Rightarrow}{\boldsymbol{\mu}}^{(\omega)}$, is positive semi-definite. Because of this, and the fact that the mobility tensor also is symmetric, there always exists an angular orientation for which $\overset{\Rightarrow}{\boldsymbol{\mu}}^{(\omega)}$ is diagonal. When both the orientation of the principal axes and the principal values of $\overset{\Rightarrow}{\boldsymbol{\mu}}^{(\omega)}$ are known, the components of tensor $\overset{\Rightarrow}{\boldsymbol{\mu}}^{(\omega)}$ for any possible angular orientation can be found using standard rotation matrix, $\overset{\Rightarrow}{\boldsymbol{\Omega}}^{(q)}$ [41, 9]

$$\overset{\Rightarrow}{\boldsymbol{\mu}}^{(\omega)} = \overset{\Rightarrow}{\boldsymbol{\Omega}}^{(q)T} \cdot \overset{\Rightarrow}{\boldsymbol{\mu}}_d^{(\omega)} \cdot \overset{\Rightarrow}{\boldsymbol{\Omega}}^{(q)}. \quad (1.1-26)$$

Subscript d denotes a diagonal tensor, and superscript (q) indicates the chosen set of generalized coordinates.

In the BD-algorithm, we need the matrix $\overset{\Rightarrow}{\boldsymbol{B}}$ defined by $\overset{\Rightarrow}{\boldsymbol{\mu}}^{(q)} = \overset{\Rightarrow}{\boldsymbol{B}} \cdot \overset{\Rightarrow}{\boldsymbol{B}}^T$. Because there always exists an orientation where $\overset{\Rightarrow}{\boldsymbol{\mu}}^{(\omega)}$ is diagonal, the following is also always valid

$$\begin{aligned} \overset{\Rightarrow}{\boldsymbol{\mu}}^{(q)} &= \overset{\Rightarrow}{\boldsymbol{\Xi}}^{(q)} \cdot \overset{\Rightarrow}{\boldsymbol{\Omega}}^{(q)T} \cdot \overset{\Rightarrow}{\boldsymbol{\mu}}_d^{(\omega)} \cdot \overset{\Rightarrow}{\boldsymbol{\Omega}}^{(q)} \cdot \overset{\Rightarrow}{\boldsymbol{\Xi}}^{(q)T} \\ &= \left[\overset{\Rightarrow}{\boldsymbol{\Xi}}^{(q)} \cdot \overset{\Rightarrow}{\boldsymbol{\Omega}}^{(q)T} \cdot \left(\overset{\Rightarrow}{\boldsymbol{\mu}}_d^{(\omega)} \right)^{1/2} \cdot \overset{\Rightarrow}{\boldsymbol{S}} \right] \cdot \left[\overset{\Rightarrow}{\boldsymbol{S}}^T \cdot \left(\overset{\Rightarrow}{\boldsymbol{\mu}}_d^{(\omega)} \right)^{1/2} \cdot \overset{\Rightarrow}{\boldsymbol{\Omega}}^{(q)} \cdot \overset{\Rightarrow}{\boldsymbol{\Xi}}^{(q)T} \right] \\ &= \left[\overset{\Rightarrow}{\boldsymbol{\Xi}}^{(q)} \cdot \overset{\Rightarrow}{\boldsymbol{\Omega}}^{(q)T} \cdot \left(\overset{\Rightarrow}{\boldsymbol{\mu}}_d^{(\omega)} \right)^{1/2} \cdot \overset{\Rightarrow}{\boldsymbol{S}} \right] \cdot \left[\overset{\Rightarrow}{\boldsymbol{\Xi}}^{(q)} \cdot \overset{\Rightarrow}{\boldsymbol{\Omega}}^{(q)T} \cdot \left(\overset{\Rightarrow}{\boldsymbol{\mu}}_d^{(\omega)} \right)^{1/2} \cdot \overset{\Rightarrow}{\boldsymbol{S}} \right]^T \end{aligned} \quad (1.1-27)$$

provided that that $\vec{\mathbf{S}}$ is an orthogonal matrix, $\vec{\mathbf{S}} \cdot \vec{\mathbf{S}}^T = \vec{\boldsymbol{\delta}}$, where $\vec{\boldsymbol{\delta}}$ is the unit matrix. In other words, there exist an infinitely large number of different values of $\vec{\mathbf{B}}$,

$$\vec{\mathbf{B}} = \vec{\boldsymbol{\Xi}}^{(q)} \cdot \vec{\boldsymbol{\Omega}}^{(q)T} \cdot \left(\vec{\boldsymbol{\mu}}_d^{(\omega)} \right)^{1/2} \cdot \vec{\mathbf{S}}, \quad (1.1-28)$$

that all yield the same macroscopic diffusion properties. Each different value of $\vec{\mathbf{B}}$ corresponds to different Brownian trajectory. However, the trajectory is still a realization of the probability distribution obtained as a solution of the corresponding Fokker-Planck equation. This is often referred to as weak equivalence between the stochastic differential equation and the Fokker-Planck equation. Applying tensor $\vec{\mathbf{S}}$ is equivalent to rotating the Wiener process. The result is also a Wiener process. We also note that, for a given choice of $\vec{\mathbf{S}}$, the tensor $\vec{\mathbf{B}}$ required in the algorithm can be acquired using simple matrix multiplication, $\mathcal{O}(2)$, instead of the Cholesky decomposition, $\mathcal{O}(3)$.

The relation between the mobility tensor and particle surface topography described above is bad news for experimentalists. When someone has experimentally determined the principal values of $\vec{\boldsymbol{\mu}}^{(\omega)}$, all that can be said about the particle is that it belongs to an infinitely large group of particles, all with different surface topographies. Additional information will always be needed in order to determine the exact geometry of the particle in the sample. But for someone testing the integrity and numerical efficiency of new algorithms, this is an ideal situation. When a test has been carried out for one set of principal values for the mobility tensor, the algorithm has in fact been tested for an infinitely larger number of surface topographies. Some of these topographies will be highly irregular, but many of these surface topographies will be highly realistic representations of biomolecules.

The arguments given above are mathematically similar to those used to describe rotational kinetic energy of rigid bodies. The rotational kinetic energy of a rigid body can be expressed in terms of only the principal values of the moment of inertia tensor. For each set of principal values of this tensor, there exist an infinitely large number of rigid bodies, all with different surface topography and mass density distributions.

Euler angles

Equation (1.1-24) is independent of the choice of generalized coordinates describing angular orientation of the particles. Apart from the metric force, only the explicit expressions for the individual matrix components of $\vec{\boldsymbol{\Omega}}^{(q)}$ and $\vec{\boldsymbol{\Xi}}^{(q)}$ will change if other choices of generalized coordinates are made.

When y -convention Eulerian angles are used to describe the orientation of the principal axes of the particle relative to the laboratory coordinate system, $\vec{\boldsymbol{\Omega}}^{(q)}$ and $\vec{\boldsymbol{\Xi}}^{(q)}$ can be

found in several textbooks on classical mechanics, e.g. Goldstein [41], and read

$$\stackrel{\Rightarrow}{\Omega}^{(\phi\theta\psi)} = \begin{pmatrix} c\psi c\theta c\phi - s\psi s\phi & c\psi c\theta s\phi + s\psi c\phi & -c\psi s\theta \\ -s\psi c\theta c\phi - c\psi s\phi & c\psi c\phi - s\psi c\theta s\phi & s\psi s\theta \\ c\phi s\theta & s\phi s\theta & c\theta \end{pmatrix} \quad (1.1-29)$$

and

$$\stackrel{\Rightarrow}{\Xi}^{(\phi\theta\psi)} = \begin{pmatrix} 0 & -s\phi & c\phi s\theta \\ 0 & c\phi & s\phi s\theta \\ 1 & 0 & c\theta \end{pmatrix}^{-1}. \quad (1.1-30)$$

In Equations (1.1-29) and (1.1-30) $s\phi$, $c\phi$ etc. denotes $\sin \phi$ and $\cos \phi$ respectively. It can be seen that tensor $\stackrel{\Rightarrow}{\Xi}^{(\phi\theta\psi)}$ is singular for $\theta = 0$ and $\theta = \pi$.

The equilibrium probability density is given by

$$p^{(\text{eq})}(\theta) \propto \sin \theta. \quad (1.1-31)$$

Cartesian components of the rotation vector

Using the Cartesian components of the rotation vector as generalized coordinates describing angular orientation gives different rotation and transformation matrices. They can be found through geometrical considerations [9, 42], and read

$$\begin{aligned} \stackrel{\Rightarrow}{\Omega}^{(a)} &= \frac{1}{\Phi^2} \begin{pmatrix} \Phi^2 \cos \Phi & -a_3 \Phi \sin \Phi & a_2 \Phi \sin \Phi \\ a_3 \Phi \sin \Phi & \Phi^2 \cos \Phi & -a_1 \Phi \sin \Phi \\ -a_2 \Phi \sin \Phi & a_1 \Phi \sin \Phi & \Phi^2 \cos \Phi \end{pmatrix} \\ &+ \frac{1 - \cos \Phi}{\Phi^2} \begin{pmatrix} a_1 a_1 & a_1 a_2 & a_1 a_3 \\ a_2 a_1 & a_2 a_2 & a_2 a_3 \\ a_3 a_1 & a_3 a_2 & a_3 a_3 \end{pmatrix} \end{aligned} \quad (1.1-32)$$

and

$$\begin{aligned} \stackrel{\Rightarrow}{\Xi}^{(a)} &= \frac{1}{2} \left[\frac{1}{\Phi^2} - \frac{\sin \Phi}{2\Phi(1 - \cos \Phi)} \right] \begin{pmatrix} a_1 a_1 & a_1 a_2 & a_1 a_3 \\ a_2 a_1 & a_2 a_2 & a_2 a_3 \\ a_3 a_1 & a_3 a_2 & a_3 a_3 \end{pmatrix} \\ &+ \begin{pmatrix} \frac{\Phi \sin \Phi}{1 - \cos \Phi} & -a_3 & a_2 \\ a_3 & \frac{\Phi \sin \Phi}{1 - \cos \Phi} & -a_1 \\ -a_2 & a_1 & \frac{\Phi \sin \Phi}{1 - \cos \Phi} \end{pmatrix}. \end{aligned} \quad (1.1-33)$$

It can readily be shown using Taylor series expansion that the tensor $\stackrel{\Rightarrow}{\Xi}^{(a)}$ exhibits no singularities in the subspace $\Phi \in [0, \pi)$.

For the general definition of the rotation vector $\vec{a} = g(\Phi)\vec{\delta}^{(a)}$, the equilibrium probability density is given by

$$p^{(\text{eq})}(\vec{a}) \propto \frac{1 - \cos \Phi}{[g(\Phi)]^2 g'(\Phi)}. \quad (1.1-34)$$

When $g(\Phi) = \Phi$, this yields [9]

$$p^{(\text{eq})}(\vec{a}) \propto \frac{1 - \cos \Phi}{\Phi^2}. \quad (1.1-35)$$

1.1.8 Metric Force

The metric force for rotational Brownian dynamics reads [6, 35, 46]

$$\vec{F}^{(\text{m,rot})} = \frac{1}{2} k_B T \frac{\partial}{\partial \vec{q}} \ln \left| \vec{\mathbf{m}}^{(\text{q,rot})} \right|, \quad (1.1-36)$$

where the generalized mass tensor $\vec{\mathbf{m}}^{(\text{q,rot})}$ is given by the following expression for the rotational kinetic energy

$$\mathcal{K} = \frac{1}{2} \dot{\vec{q}}^{(\text{rot})} \cdot \vec{\mathbf{m}}^{(\text{q,rot})} \cdot \dot{\vec{q}}^{(\text{rot})}. \quad (1.1-37)$$

The rotational kinetic energy may also be expressed as

$$\mathcal{K} = \frac{1}{2} \vec{\omega} \cdot \vec{\mathbf{m}}^{(\omega,\text{rot})} \cdot \vec{\omega}, \quad (1.1-38)$$

where $\vec{\omega}$ is the Cartesian angular velocity of the particle and the associated generalized mass tensor $\vec{\mathbf{m}}^{(\omega,\text{rot})}$ equals the moment of inertia tensor.

Using the transformation matrix $\vec{\Xi}^{(\text{q})}$ between the Cartesian angular velocities and the choice of generalized coordinate velocities we get that

$$\vec{\mathbf{m}}^{(\text{q,rot})} = \vec{\Xi}^{(\text{q})} \cdot \left(\vec{\Omega}^{(\text{q})\text{T}} \cdot \vec{\mathbf{m}}_d^{(\omega,\text{rot})} \cdot \vec{\Omega}^{(\text{q})} \right) \cdot \vec{\Xi}^{(\text{q})\text{T}}, \quad (1.1-39)$$

where $\vec{\Omega}^{(\text{q})}$ is rotation matrix in terms of the chosen generalized coordinates describing the angular orientation and $\vec{\mathbf{m}}_d^{(\omega,\text{rot})}$ is a diagonal tensor.

This shows that changing the particle mass density distribution only affects the generalized mass tensor through the numerical values of $\vec{\mathbf{m}}_d^{(\omega,\text{rot})}$, i.e. the principal values of the moment of inertia tensor.

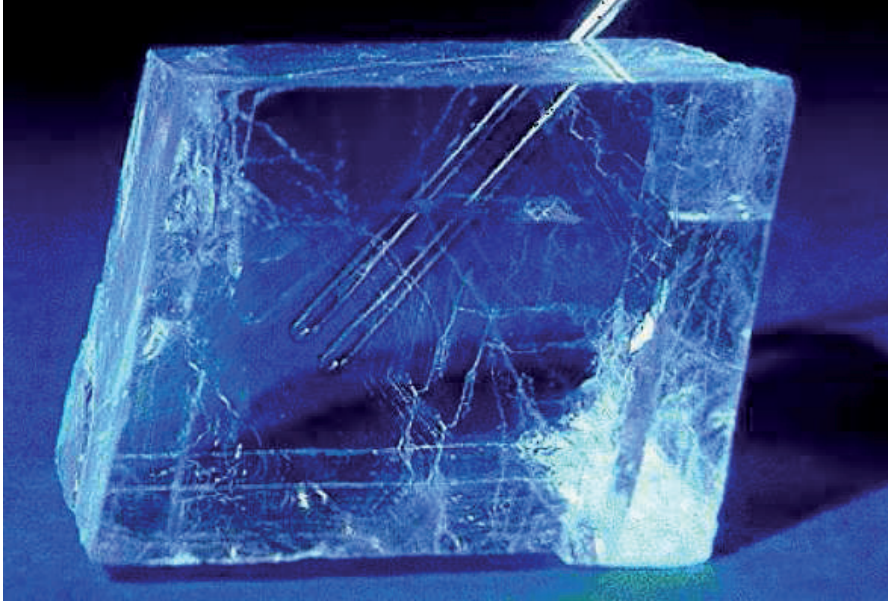


Figure 1.9: Typical example of birefringence. In this case the phenomenon is observed in a CaCO_3 -crystal.

When the y -convention Euler angles are used as generalized coordinates describing angular orientation, the analytic expressions for the metric force reads [6, 35, 46]

$$\vec{\mathcal{F}}^{(m,\phi\theta\psi)} = k_{\text{B}}T \frac{\cos \theta}{\sin \theta} \begin{pmatrix} 0 \\ 1 \\ 0 \end{pmatrix}. \quad (1.1-40)$$

This expression is singular for $\theta = 0$ and $\theta = \pi$. Instead, choosing the Cartesian components of the rotation vector yields the following expression for the metric force

$$\vec{\mathcal{F}}^{(m,a)} = k_{\text{B}}T \left[\frac{\sin \Phi}{1 - \cos \Phi} - \frac{2}{\Phi} \right] \vec{\delta}^{(a)}, \quad (1.1-41)$$

which is non-singular in the subspace used in the algorithm, $\Phi \in [0, \pi)$.

1.2 Electro-optics

The algorithms have been tested on both equilibrium and non-equilibrium systems. Transient electrically induced birefringence is the main physical phenomenon I have simulated in order to verify the output of the algorithms. Figure (1.9) shows a typical example of birefringence. In this section, a short description of the theoretical framework for transient electrically induced birefringence is given.

The Maxwell equations treat the optical medium as a continuum [47]. The displacement vector, \vec{D} , is defined as

$$\vec{D} = \epsilon_0 \vec{\mathcal{E}} + \vec{P}, \quad (1.2-1)$$

where ϵ_0 is the permittivity of vacuum, $\vec{\mathcal{E}}$ is the electric field, and \vec{P} equals the total local density of electric dipole moments. This includes both the solvent and solute molecules. The electric dipole moment of the rigid molecule ν reads

$$\vec{P}_\nu = \vec{\alpha}_\nu \cdot \vec{\mathcal{E}}, \quad (1.2-2)$$

where $\vec{\alpha}_\nu$ equals the electric susceptibility or polarization tensor of the rigid particle. The polarization tensor is positive semi-definite. This means, that for a certain angular orientation of the molecule, the polarization tensor will be diagonal. The diagonal values are referred to as the principal values of the polarization tensor, while the axes of the associated body-fixed coordinate system are referred to as the principal axes of electric polarization. For most biomolecules, the three principal values of the polarization tensor will be different. When this is the case, the molecules are said to be optically anisotropic. Combining Equations (1.2-1) and (1.2-2) yields

$$\begin{aligned} \vec{D} &= \epsilon_0 \vec{\mathcal{E}} + \langle \vec{\alpha}_\nu \rangle \cdot \vec{\mathcal{E}} \\ &= \left(\epsilon_0 \vec{\delta} + \langle \vec{\alpha}_\nu \rangle \right) \cdot \vec{\mathcal{E}} \\ &= \vec{\epsilon} \cdot \vec{\mathcal{E}}, \end{aligned} \quad (1.2-3)$$

where $\langle \dots \rangle$ denotes the ensemble average, and $\vec{\epsilon}$ is the permittivity tensor. For systems in thermal equilibrium, $\vec{\epsilon} = \epsilon_0 \vec{\delta}$ even when the system contains a multitude of different optically anisotropic particles.

Most large biomolecules have several fixed electrically charged groups on the surface. Normally, this also means that these molecules have an associated permanent electric dipole moment. The presence of an external electric field will then give rise to a torque on the particle and an associated new equilibrium probability density in the molecule angular coordinate space. When this is true, the principal values of $\vec{\epsilon}$ will no longer be the same. As a result, the optical properties of the solution will depend on both the direction and the polarization of the beam of light that passes through specimen. In such cases, the Maxwell equations yield that the phase velocity of two light beams with orthogonal polarization will in general be different. This is referred to as optical birefringence.

In addition, large biomolecules have often so called electrically induced dipole moments. These dipole moments are highly influenced by an external electric field. As for permanent electric dipole moments, the induced dipole moments also give rise to a torque. This torque is caused by the same external electric field. The induced dipole moments will in turn have an influence on the equilibrium probability density, which consequently affects the optical birefringence.

Most biomolecules exhibit larger polarizability at low frequencies than at optical frequencies. In measurements of electrically induced birefringence the rise and fall time of the external electric field pulses can be in the nanosecond range. This means that, for these types of experiments, the characteristic frequency components of the external field pulses

are in the GHz range. Optical frequencies are typically about 500000 GHz. The expression for the electric dipole induced by the external field is analogous to those for optical frequencies, but the numerical values will in general be different

$$\vec{P}_\nu = \vec{\alpha}_{0,\nu} \cdot \vec{\mathcal{E}}, \quad (1.2-4)$$

where $\vec{\alpha}_{0,\nu}$ often is often referred to as the "low-frequency" electric susceptibility. The dipole moment induced by the external electric field pulse contributes to the alignment of the molecules parallel to the external electric field, and thus the stationary birefringence of the sample. The principal axes of the "low-frequency" polarization tensor will in general not coincide with the principal axes of the susceptibility tensor at optical frequencies.

The phase velocity of a light beam is inversely proportional to the index of refraction. The birefringence of the macromolecular solution is defined as

$$\Delta n = n_{\parallel} - n_{\perp}, \quad (1.2-5)$$

where n_{\parallel} and n_{\perp} are the indices of refraction for light polarized in directions parallel and perpendicular to the external electric field, respectively.

For particles with elongated shape it can be shown [48, 49, 50] that, when an external electric field is applied, the rise of the time-dependent relative birefringence reads

$$\frac{\Delta n(t)}{\Delta n_0} = 1 - \frac{3p^2/q}{2(p^2/q + 1)} \exp(-2D_R t) + \frac{p^2/q - 2}{2(p^2/q + 1)} \exp(-6D_R t). \quad (1.2-6)$$

Here, t is time, Δn_0 is the stationary birefringence level, p and q are the dimensionless permanent and induced dipole moments, respectively, and D_R is the macroscopic rotational diffusion coefficient. For a symmetric reversing electric pulse, when the reverse electric field is applied, the time-dependent relative birefringence is given as

$$\frac{\Delta n(t)}{\Delta n_0} = 1 - \frac{3p^2/q}{p^2/q + 1} [\exp(-2D_R t) - \exp(-6D_R t)]. \quad (1.2-7)$$

In Equations (1.2-6) and (1.2-7), the dimensionless permanent and induced dipole moments are defined as $p := \mu_p \mathcal{E} / (k_B T)$ and $q := (\alpha_z - \alpha_x) \mathcal{E}^2 / (k_B T)$. The permanent electric dipole moment equals μ_p , and the induced electric dipole moment equals the difference between the polarizabilities α_x and α_z along the particle axes x and z , respectively. The parameter \mathcal{E} is the amplitude of the external electric field. Equations (1.2-6) and (1.2-7) are both exact in the limit $p \rightarrow 0$ and $q \rightarrow 0$. For constant non-zero electric fields these equations provide accurate estimates of the birefringence only as long as p and q both are much smaller than 1.

When the external electric field is abruptly turned off, the behavior of the time-dependent relative birefringence becomes the well-known free decay process

$$\frac{\Delta n(t)}{\Delta n_0} = \exp(-6D_R t). \quad (1.2-8)$$

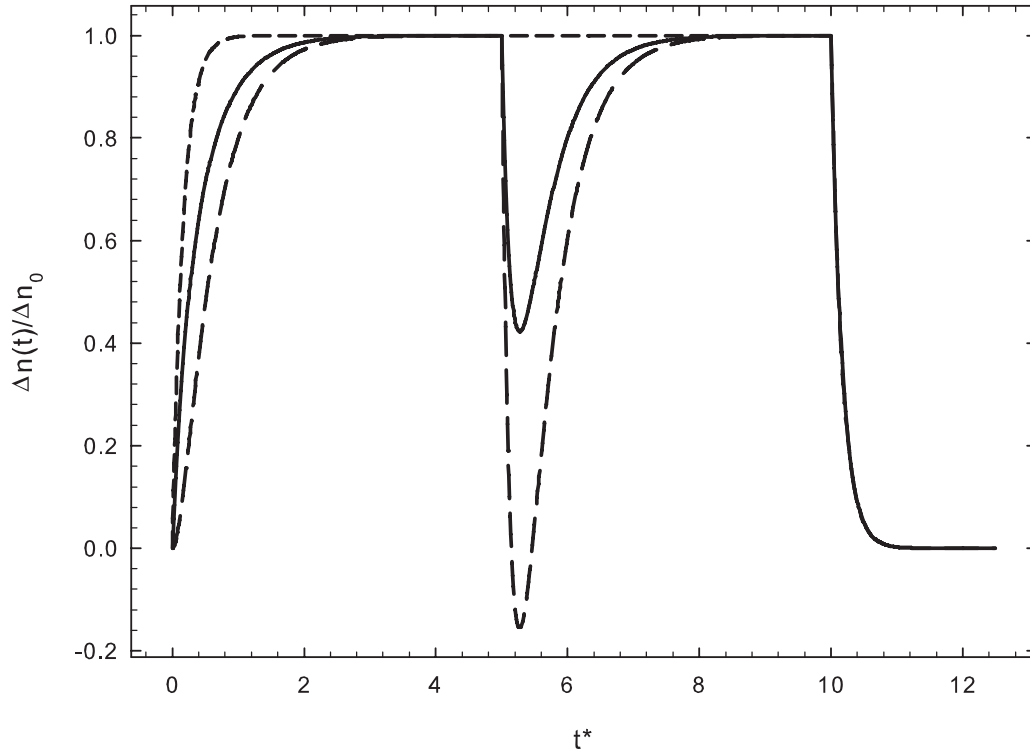


Figure 1.10: Theoretical time-dependent relative birefringence. Dimensionless time $t^* = D_R t$ is used. The system is exposed to one symmetric reversing electric pulse. At time $t^* = 0$, the electric field is switched on, and at time $t^* = 5$ the direction of the electric field is reversed. At time $t^* = 10$, the electric field is switched off. Dashed line: Pure permanent dipole moment ($p = 1.0, q = 0.0$). Short dashed line: Pure induced dipole moment ($p = 0.0, q = 1.0$). Solid line: Combination of permanent and induced dipole moments ($p = 1.0, q = 1.0$).

For rigid particles with other surface topographies, the equations (1.2-6-1.2-8) assume a different form. For example, the decay process is thoroughly studied by Favro [27] and Wegener [51]. Figure (1.10) shows the theoretical time-dependent birefringence when three different systems are exposed to two electric pulses with opposite polarity. Because of a relatively low signal-to-noise ratio in the simulation results when p and q are very small, we have for practical reasons studied systems where p and q are slightly larger than the theoretical recommendations. The theoretical curves are obtained for particles with pure permanent dipole moment ($p = 1.0, q = 0.0$), particles with pure induced dipole moment ($p = 0.0, q = 1.0$), and particles with both permanent and induced dipole moments ($p = 1.0, q = 1.0$). The electric field is switched on at time $t = 0$, and at time $t = 5$ the direction of the electric field is reversed. Finally, following the electric field being switched off at time $t = 10$, the system approaches equilibrium where the birefringence is 0.

The stationary birefringence level, Δn_0 , follows the Kerr law when the potential energy of the dipole moment in the external electric field is less than the thermal energy (the thermal regime)

$$\Delta n_0 = K \lambda_0 \mathcal{E}^2. \quad (1.2-9)$$

Here K is the Kerr constant and λ_0 is the wavelength of the light passing through the system. At high electric field strengths, the molecules orient themselves parallel to the electric field and a saturation level, Δn_s , is observed. In the thermal regime, the steady state is described by

$$\lim_{\mathcal{E} \rightarrow 0} \frac{\Delta n_0}{\mathcal{E}^2} = \frac{\Delta n_s}{15\mathcal{E}^2} (p^2 + q). \quad (1.2-10)$$

This expression provides a relation between the saturation level and the thermal regime stationary birefringence level, and can be used when the wavelength and the Kerr constant are unknown.

Chapter 2

Concluding remarks and future perspective

This thesis has brought the plan consisting of 6 steps described early in chapter 1 closer to completion. Steps 1 and 2 were completed in the previous works [8] and [9, 10]. Steps 3 and 4 have been addressed by the current thesis. The work on steps 5 and 6 has been initiated and has in part been completed, but still there remains some work before the long term goal has been reached.

Generalized coordinates have been used, rather than other common parameterizations of angular orientation. This ensures that the algorithm yields equilibrium probability densities that are in agreement with the generalized Boltzmann equilibrium probability densities. Also, the algorithm will at all times produce results consistent with the fluctuation dissipation theorem.

We have devised a method for comparing the computational efficiency of Brownian dynamics algorithms using different generalized coordinates describing angular orientation. The method is independent of the particle mobility tensor, which means that the calculation of this tensor can be performed in a pre-calculation step. This leaves the algorithms themselves unaffected, and the simulations become computationally highly efficient. The mobility tensor itself can be obtained using already existing methods.

Two choices of generalized coordinates describing angular orientation have been compared: the Euler angles and the Cartesian components of the rotation vector. The corresponding algorithms both yield results in agreement with theory as long as the numerical time steps are small enough. However, as predicted by the theoretical work, the Cartesian components of the rotation vector prove to be more efficient because of the non-singular expressions. We have shown that the relative computational efficiency depends on the physical conditions imposed on the simulations. In extreme non-equilibrium situations, we have observed a factor 10^3 in favor of the Cartesian components of the rotation vector.

In order to compare the algorithms, the nanoparticle systems have been kept as simple as possible. Consequently, the simulations made in this thesis only involve single rigid particles with arbitrary surface topographies, for which we have shown that the results are in accordance with theoretical predictions. Such particles are commercially available, i.e. proteins, DNA, and RNA. The particular case when translational motion can be ignored, and thus no coupling between translational and rotational motion, has, in this thesis, thoroughly been studied. To achieve a complete understanding of Brownian dynamics in nanoparticle systems, however, coupling between translational and rotational motion is required. It is also necessary to take into account chains of arbitrarily shaped particles. The theory exists, and already most of the foundations have been implemented. The inter-particle constraints or forces, i.e. interconnecting springs or excluded volume, remain.

As stated at the beginning of this text, our long term goal is to obtain predictions from simulations and experiments that are one order of magnitude more precise than the current standard. Substantial progress has been made toward this goal, as now the non-singular behavior of the Cartesian components of the rotation vector, and the consistency of our rotational dynamics engine, have both been verified. The simulation tool to obtain such predictions is therefore much closer to completion. We are aware, however, that a large amount of work still remains and most likely, unexpected hurdles will appear along the road. The next natural step is to integrate the rotational dynamics engine into the complete Brownian dynamics algorithm, which includes translation and rotation of N arbitrarily shaped particles linked together as a polymer, and where complete fluid dynamic interaction between any particle pair is included.

When all the 6 steps are completed and our long term goal is achieved, it will represent a major scientific step forward. We will then be able to compare quantitative simulation results and high-quality experimental data. From this detailed comparison, we expect to extract new important information about nanoparticle systems, and it will be possible to provide detailed answers to many of the so far unanswered fundamental questions related to nanoparticle dynamics.

Chapter 3

Summary of papers

Paper I [1]:

We compare the two sets of generalized coordinates, the Euler angles and the Cartesian components of the rotation vector, and describe their advantages and disadvantages. This is done with respect to diffusion equations and analytical expressions of electro-optics. We also show that, in a special case, the generalized force associated with Cartesian components of the rotation vector equals the torque. In addition, we introduce a new graphical approach to quantitatively track how changes in the Euler angles affect the rotation vector.

Paper II [2]:

We demonstrate a new Brownian dynamics algorithm that can be used to study free rotational diffusion of rigid particles with arbitrary surface topography. The only parameters dependent on particle shape are the three principal values of the rotational mobility tensor. These three scalars contain all information about the surface topography relevant for particle rotational diffusion. The algorithm is highly efficient because the principal values of the rotational mobility tensor only need to be pre-calculated once. In this paper, the Euler angles are used as generalized coordinates describing angular orientation.

Paper III [3]:

We present the first report on the merit of using the Cartesian components of the rotation vector as generalized coordinate describing angular orientation in Brownian dynamics simulations. This choice of coordinates is compared to the use of the standard choice of coordinates, the Euler angles. We find that the Cartesian components of the rotation vector, in some cases, yield more than a 1000-fold increase in computational efficiency.

Paper IV [4]

We study the transient electrically induced birefringence in dilute solutions of rigid particles in response to external electric field pulses. This is achieved using our new Brownian dynamics algorithm rigorously derived from kinetic and stochastic theory. Both one single electric pulse and two electric pulses with opposite polarity are being analyzed. We

document that our singularity-free algorithm performs flawlessly, and that it in general outperforms algorithms based on the Euler angles.

References

- [1] T.R. Evensen, A. Elgsaeter, and S.N. Naess, *Colloids and Surfaces B: Biointerfaces*, **56**, 80, (2007).
- [2] T.R. Evensen, S.N. Naess, and A. Elgsaeter, *Macromol. Theory Simul.*, **17**, 121, (2008).
- [3] T.R. Evensen, S.N. Naess, and A. Elgsaeter, *Macromol. Theory Simul.*, (2008), accepted.
- [4] T.R. Evensen, S.N. Naess, and A. Elgsaeter, *Macromol. Theory Simul.*, (2008), submitted.
- [5] R.B. Bird, C.F. Curtiss, R.C. Armstrong, and O. Hassager, *Dynamics of Polymeric Liquids, Vol.2, Kinetic Theory*, 2nd ed. (Wiley, New York, 1987).
- [6] H.C. Öttinger, *Stochastic Processes in Polymeric Fluids* (Springer, Berlin, 1996).
- [7] S.N. Naess, H.M. Adland, A. Mikkelsen, and A. Elgsaeter, *Physica A* **294**, 323 (2001).
- [8] S.N. Naess and A. Elgsaeter, *Macromol. Theory Simul.* **11**, 913 (2002).
- [9] S.N. Naess, A. Elgsaeter, *Macromolecular Theory and Simulations*, **13** 419 (2004).
- [10] S.N. Naess, A. Elgsaeter, *Macromolecular Theory and Simulations*, **14** 300 (2005).
- [11] P.W. Van der Pas, *Gillispie CC (ed) Dictionary of Scientific Biography Vol VII*, (C Shribner's Sons, New York, 1973)
- [12] R. Brown, *Phil. Mag.* **4**, 161 (1828).
- [13] A. Einstein, *Ann. Phys.* **17**, 549 (1905).
- [14] P. Langevin, *Compendes Rendus Acad. Sci. (Paris)*, **146**, 530 (1908).
- [15] D.S. Lemons and A. Gythiel, *Am. J. Phys.* **65**, 1079 (1997).
- [16] R. Zwanzig, *Adv. Chem. Phys.* **15**, 325 (1969).
- [17] M. Fixman, *J. Chem. Phys.* **69**, 1527 (1978).

- [18] M. Fixman, J. Chem. Phys. **69**, 1538 (1978).
- [19] D.L. Ermak and J.A. McCammon, J. Chem. Phys. **69**, 1352 (1978).
- [20] H.A. Kramers, Physica **11**, 1 (1944). English translation: J. Chem. Phys. **14**, 415 (1946).
- [21] P.E. Jr Rouse, J. Chem. Phys. **21**, 1272 (1953).
- [22] B.H. Zimm, J. Chem. Phys. **24**, 269 (1956).
- [23] J.G. Kirkwood, *Macromolecules* (Gordon and Breach, New York, 1967).
- [24] H.R. Jr Warner, Ind. Eng. Chem. Fund. **11**, 379 (1972).
- [25] P. Debye, *Polar Molecules* (Chemical Catalog Co, New York, 1929)
- [26] F. Perrin, J. Phys. Radium **5**, 497, (1934)
- [27] L. D. Favro, Phys. Rev. , **119**, 53, 1960.
- [28] M.P. Allen and D.J. Tildesley, *Computer Simulation of Liquids* (Clarendon, Oxford, 1989).
- [29] S.A. Allison and J.A. McCammon, Biopolymers **23**, 167 (1984).
- [30] H.C. Öttinger, Phys. Rev. E. **50**, 2696 (1994).
- [31] J. Antosiewicz, T. Grycuk, and D. Porschke, J. Chem. Phys. **95**, 1354 (1991).
- [32] J. Garcia de la Torre, Eur. Biophys. J. **23**, 307 (1994).
- [33] G.H. Nyland, P. Skjetne, A. Mikkelsen, and A. Elgsaeter, J. Chem. Phys. **105**, 1198 (1996).
- [34] P. Skjetne and A. Elgsaeter, Comput. Theor. Polym. Sci. **9**, 153 (1999).
- [35] A. Mikkelsen , K.D. Knudsen, and A. Elgsaeter, Physica A **253**, 66 (1998).
- [36] E. Klaveness and A. Elgsaeter, J. Chem. Phys. **110**, 11608 (1999).
- [37] S.A. Allison and J.A. McCammon, Biopolymers **23**, 167 (1984)
- [38] S. A. Allison, Macromolecules **24**, 530 (1991)
- [39] M. X. Fernandes and J. G. de la Torre, Biophys. J., **83**, 3039 (2002).
- [40] D. A. Beard and T. Schlick, Biophys. J., **85**, 2973 (2003).
- [41] H. Goldstein, *Classical Mechanics*, 2nd ed. (Addison-Wesley, Reading, MA, 1980).
- [42] O.A. Bauchau, L. Trainelli, Nonlinear Dynamics, 32 (2003) 71.

- [43] H. Risken, *The Fokker-Planck Equation. Methods of Solution and Applications*, 2nd ed. (Springer, Berlin, 1989).
- [44] R. Kubo, M. Toda, and N. Hashitsume, *Statistical Physics II, Nonequilibrium Statistical Mechanics* (Springer, Berlin, 1985).
- [45] R.B. Bird, C.F. Curtiss, R.C. Armstrong, and O. Hassager, *Dynamics of Polymeric Liquids, Vol.1, Fluid Mechanics*, 2nd ed. (Wiley, New York, 1987).
- [46] D.C. Morse, *Adv. Chem. Phys.*, **2004**, 128, 65.
- [47] M. Born and E. Wolf, *Principles of Optics*, 7th ed. (Cambridge University Press, Cambridge, 1999).
- [48] E. Fredricq and C. Houssier, *Electric Dichorism and Electric Birefringenc*, (Clarendon Press, Oxford, 1973).
- [49] A. Bjorkoy, A. Elgsaeter, and A. Mikkelsen, *Biophys. Chem.* **72**, 247, 1998.
- [50] I. Tinoco, *J. Am. Chem. Soc.* , **77**, 4486, 1955.
- [51] W. A. Wegener, *Journal of Chemical Physics* , **70**, 633, 1979.

Appendix A

Collection of papers

Paper I



Transient molecular electro-optics Cartesian rotation vector versus Eulerian angles

Tom Richard Evensen, Arnljot Elgsaeter, Stine Nalum Naess*

*Department of Physics, Norwegian University of Science and Technology (NTNU),
Høgskoleringen 5, 7491 Trondheim, Norway*

Available online 20 December 2006

Abstract

Comparing the Euler angles, the classical choice of generalized coordinates describing the three rotational degrees of freedom of a rigid body, and the Cartesian rotation vector, we show that they both have their advantages and disadvantages in kinetic theory and Brownian dynamics analysis of molecular electro-optics. The Eulerian angles often yield relatively simple, yet singular, equations of motion, while their counterparts expressed in terms of Cartesian rotation vector are non-singular but more complex. In a special case, we show that the generalized force associated with the Cartesian rotation vector equals the torque. In addition, we introduce a new graphical approach to qualitatively track how changes in the Eulerian angles affect the Cartesian rotation vector.

© 2006 Elsevier B.V. All rights reserved.

Keywords: Molecular electro-optics; Cartesian rotation vector; Eulerian angles; Brownian dynamics; Theory

1. Introduction

Measuring the response to changes in external electric fields constitutes an important method for determining nanoparticle, or macromolecular, structure and function. Studies of electro-optic phenomena, such as electrically induced birefringence, are usually performed without much consideration given to the choice of generalized coordinates employed to specify the angular orientation of the macromolecules. Depending on the nature of the studies, this choice can, however, be important. The classical choice of generalized coordinates for this task is the Eulerian angles. But the Cartesian rotation vector offers an interesting alternative set of generalized coordinates. Euler fathered the theoretical foundation of also the latter choice of generalized coordinates, and it has lately been successfully employed in a several fields, such as robotics [1], aerospace engineering [2], and astronomical sciences [3]. The authors Naess and Elgsaeter [4,5] use this set of generalized coordinates to formally derive the conformation space diffusion equations from kinetic theory. They proceed by employing the equiva-

lent stochastic differential equations as a base for a Brownian dynamics algorithm for chains with and without holonomic constraints.

In this paper, we compare the two choices, Eulerian angles and Cartesian rotation vector, and explore some of their advantages and disadvantages. We find that, in molecular electro-optics analysis, the Eulerian angles often produce relatively simple analytical expressions. Most often, however, these expressions are singular. Cartesian rotation vector, on the other hand, yields quite opposite results—complex, but non-singular analytical expressions. In a special case, we show that the conjugated generalized force of the Cartesian rotation vector simply equals the torque. This is employed to extract information about the mobility tensor of a rigid body.

2. Eulerian angles

The classical and most common choice of generalized coordinates used to describe the angular orientation of a rigid body relative to the laboratory coordinate system is the Eulerian angles. In this text, we will only consider *y*-convention Eulerian angles, but the principles described and arguments given here apply to other conventions as well. The *y*-convention Eulerian angles are ϕ , θ , and ψ as shown in Fig. 1.

* Corresponding author. Tel.: +47 73593435; fax: +47 73597710.
E-mail address: Stine.Naess@phys.ntnu.no (S.N. Naess).

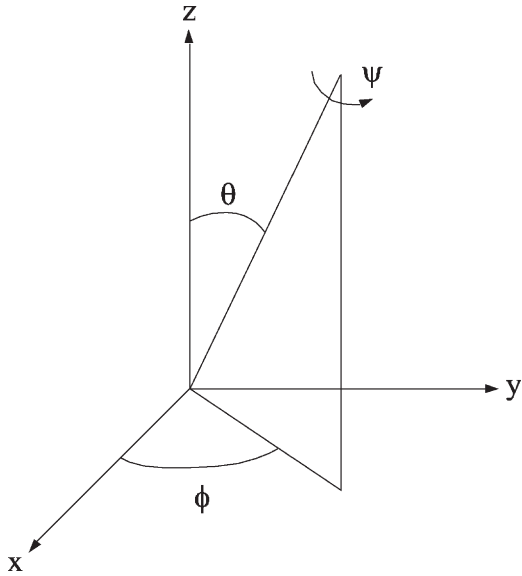


Fig. 1. Schematic illustration of the y-convention Eulerian angles. The sequence of rotations is ϕ , θ , and ψ .

2.1. Analytical expressions

What are the attractive features of the Eulerian angles that have made them so popular over the years? One major advantage of using Eulerian angles in molecular electro-optics, is that many important relations turn out to be functions of only one of the Eulerian angles: θ . This analytical simplicity does not appear, as will be seen, for other choices of generalized coordinates such as the Cartesian components of the rotation vector.

For example, consider an ellipsoidal rigid nanoparticle with permanent electric dipole moment aligned along the axis of rotational symmetry. The electric polarizability is assumed to be homogeneous through out the nanoparticle. Then, the polar angles ϕ and θ , a subset of the Eulerian angles, suffice to represent its orientation. In this case, the potential energy of the dipole in an external electric field depends only on the angle θ

$$V(\theta) = -\mu E \cos \theta - \frac{1}{2}v(\hat{\alpha}_1 \cos^2 \theta + \hat{\alpha}_2 \sin^2 \theta)E^2, \quad (1)$$

where \vec{E} is the external electric field, μ the permanent dipole moment, and v is the volume of the body [6]. The parameters $\hat{\alpha}_1$ and $\hat{\alpha}_2$ are the electrical polarizabilities per unit volume when the electric field is parallel and perpendicular to the axis of rotational symmetry, respectively. The first term is associated with the permanent dipole moment, while the second is due to the induced dipole moment.

Another example of an important relation expressed in terms of only one of the Eulerian angles is the total birefringence of a homogenous solution or a suspension of nanoparticles [7]

$$\Delta n = \frac{Nv(\hat{\alpha}_1 - \hat{\alpha}_2)}{2n_0\epsilon_0} \int_0^\pi 2\pi \sin \theta P_2(\cos \theta) f(\theta) d\theta, \quad (2)$$

where N is the number of particles per volume, n_0 the refractive index of the solution, ϵ_0 the permittivity of vacuum, and $P_2(u)$ is the second Legendre polynomial $P_2(u) = (3u^2 - 1)/3$. The to-

tal birefringence is also a function of θ alone. The mathematical expression for the dichroism of a solution/suspension is similar, but this will not be considered here.

The conformation angular diffusion equation [8] shows singular behavior for $\theta = 0$ and $\theta = \pi$, but still has a relatively simple analytical form

$$\frac{1}{D^{(R)}} \frac{\partial \Psi}{\partial t} = \frac{1}{\sin \theta} \frac{\partial}{\partial \theta} \left(\sin \theta \frac{\partial \Psi}{\partial \theta} \right) + \frac{1}{\sin^2 \theta} \frac{\partial^2 \Psi}{\partial \phi^2}, \quad (3)$$

where $D^{(R)}$ is the rotational diffusion coefficient, $p(\vec{q}, t)$ the probability density in conformation space, and $\Psi(\vec{q}, t) = p(\vec{q}, t)/\sin \theta$.

All the examples above demonstrate the analytical simplicity that the use of Eulerian angles often offers. In order to numerically simulate the diffusion described by Eq. 3, we employ Brownian dynamics analysis. In the next section, we will present some of the results from the Brownian dynamics analysis, and also consider some of the other consequences of choosing the Eulerian angles as the generalized coordinates.

2.2. Brownian dynamics analysis

We start the derivation of some aspects of the Brownian dynamics formalism from the equilibrium probability density in phase space. For any choice of generalized coordinates, \vec{q} , and conjugated momenta, \vec{p} , the equilibrium probability density in phase space reads

$$p^{(eq,pq)}(\vec{p}, \vec{q}) = \frac{\exp\{-H(\vec{p}, \vec{q})/(k_B T)\}}{\iint \exp\{-H(\vec{p}, \vec{q})/(k_B T)\} d\vec{p} d\vec{q}}, \quad (4)$$

where k_B is the Boltzmann constant, and T is the absolute temperature. The Hamiltonian equals

$$H(\vec{p}, \vec{q}) = \frac{1}{2} \sum_s \sum_t [\vec{m}^{(q)}]_{st}^{-1} p_s p_t + \Phi(\vec{q}), \quad (5)$$

where $\vec{m}^{(q)}$ is the generalized mass tensor, and $\Phi(\vec{q})$ is the potential energy. Contraction of Eq. (4) over the momentum part of the phase space and assuming thermal equilibrium in this part of the phase space, yield the following conformation space probability density [9,10]

$$\begin{aligned} p^{(eq,q)}(\vec{q}) &= \frac{\exp\{-\Phi(\vec{q})/(k_B T)\} |\vec{m}^{(q)}|^{1/2}}{\int \exp\{-\Phi(\vec{q})/(k_B T)\} |\vec{m}^{(q)}|^{1/2} d\vec{q}} \\ &= \frac{\exp\{-[\Phi(\vec{q}) + \Phi^{(m)}(\vec{q})]/(k_B T)\}}{\int \exp\{-[\Phi(\vec{q}) + \Phi^{(m)}(\vec{q})]/(k_B T)\} d\vec{q}}. \end{aligned} \quad (6)$$

In the last part of Eq. (6), we have introduced the potential

$$\Phi^{(m)}(\vec{q}) := -\frac{1}{2} k_B T \ln |\vec{m}^{(q)}|. \quad (7)$$

This new potential corresponds to the force

$$\vec{F}^{(m)} := \frac{\partial \Phi^{(m)}(\vec{q})}{\partial \vec{q}}, \quad (8)$$

which is commonly referred to as the metric force. Using Eulerian angles to describe the angular orientation of a rigid body,

the components of the vector $\vec{r}^* = \{\vec{r}^{(\text{trans})}, \phi, \theta, \psi\}$ constitute the full set of generalized coordinates. The generalized coordinates for the rigid body center of mass are denoted $\vec{r}^{(\text{trans})}$. In this case, the metric force reads [11]

$$\vec{F}^{*(\text{m})} = k_{\text{B}} T \frac{\cos \theta}{\sin \theta} \begin{pmatrix} 0 \\ 0 \\ 0 \\ 0 \\ 1 \\ 0 \end{pmatrix}, \quad (9)$$

which is singular for $\theta = 0$ and $\theta = \pi$. It is interesting to note that the metric force, $\vec{F}^{*(\text{m})}$, appears as a consequence of contraction of the momentum space, yet $\vec{F}^{*(\text{m})}$ is a function of θ alone, and not of ϕ and ψ . Here, the generalized coordinates and conjugated momenta are per definition treated as independent variables.

The mobility tensor, $\vec{\mu}^{(q)}$, is defined by

$$\dot{\vec{q}} := \vec{\mu}^{(q)} \vec{F}^{(q)}, \quad (10)$$

where $\vec{F}^{(q)}$ is the generalized force associated with the choice of generalized coordinates. When Eulerian angles are used to describe the orientation of principal axes of the rotational mobility tensor relative to the laboratory coordinate system, the mobility tensor is singular for $\theta = 0$ and $\theta = \pi$. Naess et al. [12] show that, for the special case when the first two principal values of the rotational mobility tensor are equal, $\mu_{11}^{\text{RR}} = \mu_{22}^{\text{RR}}$, the rotational mobility tensor reads

$$\vec{\mu}^{\Rightarrow(\text{RR}, \phi\theta\psi)} = \begin{pmatrix} \frac{\mu_{11}^{\text{RR}}}{\sin^2 \theta} & 0 & \frac{-\mu_{11}^{\text{RR}} \cos \theta}{\sin^2 \theta} \\ 0 & \mu_{11}^{\text{RR}} & 0 \\ \frac{-\mu_{11}^{\text{RR}} \cos \theta}{\sin^2 \theta} & 0 & \frac{\mu_{33}^{\text{RR}} + \mu_{11}^{\text{RR}} \cos^2 \theta}{\sin^2 \theta} \end{pmatrix}. \quad (11)$$

The singularities described above give rise to several difficulties when the Eulerian angles are used as generalized coordinates in numerical simulations. One standard technique used to reduce some of these difficulties is to decrease the size of the simulation time steps. If the time steps used in the simulations are too large, the numerics tend to go astray and the results become less valuable. Use of too small time steps, on the other hand, sharply reduces the efficiency of the algorithm. Finding the right balance is therefore an important task, but not always a simple one. Due to the singular mobility tensor, one may also experience that a rigid body, e.g. make excessive jumps in conformation space even for small numerical time step. As a consequence, caution must continuously be taken when determining the correct quadrant of the Eulerian angles.

2.3. Generalized force

The generalized force was introduced in Eq. (10). We will in this section explore this force further.

Suppose that the rigid body has an ellipsoidal shape and that the generalized velocities, $\dot{\phi}$, $\dot{\theta}$, and $\dot{\psi}$, are constant. From classical mechanics [13], the generalized force is then defined as

$$\vec{F}^{(q)} = \frac{\partial(\mathcal{K} - V)}{\partial \vec{q}}, \quad (12)$$

where \mathcal{K} and V are the kinetic and potential energies, respectively. For simplicity, we assume that the body is located in a potential free environment, $V = 0$. Generally, the kinetic energy is given by

$$\mathcal{K} = \frac{1}{2} \dot{\vec{q}}^{\text{T}} \vec{m} \dot{\vec{q}}. \quad (13)$$

It can readily be verified that the kinetic energy of the ellipsoidal body equals

$$\mathcal{K} = \frac{1}{2} [I_1 \dot{\theta}^2 + (I_1 \sin^2 \theta + I_3 \cos^2 \theta) \dot{\phi}^2 + 2I_3 \cos \theta \dot{\phi} \dot{\psi} + I_3 \dot{\psi}^2], \quad (14)$$

where the elements of the diagonal inertia tensor are (I_1, I_1, I_3) . For point masses, we have that $\partial \mathcal{K} / \partial \vec{q} = \vec{0}$. In our case the coordinate dependent mass tensor yields the kinetic energy in Eq. (14). It follows, that the conjugated generalized force for Eulerian angles in the absence of external forces ($V = 0$) reads

$$\vec{F}^{(\phi\theta\psi)} = \begin{pmatrix} 0 \\ \dot{\phi}^2 (I_1 - I_3) \sin \theta \cos \theta \\ 0 \end{pmatrix}. \quad (15)$$

Here we have ignored the term containing $\dot{\phi} \dot{\psi}$, as this term vanishes during averaging.

We observe from several of the equations in this and the previous sections that $\sin \theta$ is a common factor for this choice of generalized coordinates, and that singularities frequently appear. In the next section, we take a closer look at some of the consequences of this factor and investigate the singularities.

2.4. The singularities accompanying Eulerian angles

As we have seen, the use of Eulerian angles results in singular equations of diffusion dynamics. In kinetic theory, the Eulerian angles form an orthonormal set of coordinates, just like any other set of generalized coordinates. Therefore, this cannot be the reason for these singularities. We now investigate some of these difficulties.

When viewing the Eulerian angles as regular Cartesian coordinates in a Euclidean three-dimensional space, the ranges of ϕ , θ , and ψ form a cuboid. For the planes $\theta = 0$ and $\theta = \pi$, however, this choice of generalized coordinates degenerates, as there exist an infinite number of configurations that correspond to these two θ -angles.

For a rigid body of ellipsoidal form, the polar angles (ϕ, θ) fully describe the orientation of the body. This is a simplification compared to using the complete set of Eulerian angles, but the observations that follow are similar in both cases. The kinematical metric for this choice of generalized coordinates reads

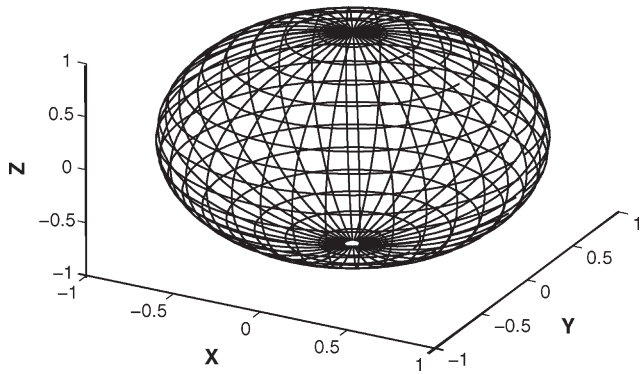


Fig. 2. Schematic illustration of the singularities at the poles that accompanies the Eulerian angles.

$$\begin{aligned} (ds)^2 &= (dx)^2 + (dy)^2 + (dz)^2 = (d\theta)^2 + \sin^2 \theta (d\phi)^2 \\ &= \begin{pmatrix} d\phi \\ d\theta \end{pmatrix}^T \begin{pmatrix} \sin^2 \theta & 0 \\ 0 & 1 \end{pmatrix} \begin{pmatrix} d\phi \\ d\theta \end{pmatrix}. \end{aligned} \quad (16)$$

We observe that the space curvature is proportional to $\sin \theta$. Studying Fig. 2 we observe that the kinematical metric in Eq. (16) becomes very small for a constant θ ($d\theta = 0$) close to the pole ($\theta = \epsilon \ll 1$). When $ds \rightarrow 0$, the velocity also exhibits the same behavior, $\dot{s} = ds/dt \rightarrow 0$. After dividing Eq. (16) by $(dt)^2$, it follows that the velocity has the same form as the kinetic energy in Eq. (13). It can be shown that the determinant of the mass tensor in Eq. (13) is $|\vec{m}^{(q)}| \propto \sin^2 \theta$, which is proportional to the curvature squared. The kinetic energy forms a complete metric in this space. But, changing the angular velocities would not change the kinetic energy for configurations where θ is close to 0. In our case, however, the mass is not a point mass, but rather coordinate dependent. As seen from Eqs. (7) and (8), this gives rise to the singular metric force, which in the diffusion equation forms a particle flux radially from each of the two poles.

A different approach to characterizing the Eulerian angles consists of observing the surface integral

$$A = \iint dx dy = \iint |J| d\phi d\theta, \quad (17)$$

where J is the Jacobi determinant. The absolute value of the Jacobi determinant in this case is well known

$$|J| = \sin \theta. \quad (18)$$

The Jacobi determinant has many interpretations [14], one of which is the volume of a parallelepiped in n -dimensional space. This volume is most often seen as a factor in the infinitesimal volume element in multiple integrals. Near the poles, $\theta = 0$ or $\theta = \pi$, this volume is close to 0, and the surface integral (17) vanishes, even when taking large ϕ -steps.

3. Rotation vector

We observed in the previous section that the Eulerian angles resulted in relatively simple analytical expressions for both the potential energy of a dipole in Eq. (1) and the total birefringence in Eq. (2). As we will show, this is not the case for the Carte-

sian rotation vector. But first, we give a short introduction to vector parameterization of angular orientation and the Cartesian rotation vector.

3.1. Vector parameterization

The rotation vector is a vector parameterization of rigid body rotation that originates from Euler. Vector parameterizations of rotation form a general class of techniques based on a minimal set of parameters. This set consists of the pair $(p, \vec{\delta}^{(a)})$, where $p = p(\Phi)$ is the generating function of the parameterization and Φ is the rotation angle about the unit vector of the axis of rotation $\vec{\delta}^{(a)}$. The generating function must be an odd function Φ , and have the limit behavior

$$\lim_{\Phi \rightarrow 0} \frac{p(\Phi)}{\Phi} = \kappa, \quad (19)$$

where Φ is a real normalization factor. Bauchau and Trainelli [2] presents a number of generating functions, including $p(\Phi) = \Phi$. Naess and Elgsaeter [4,5] uses this choice of parameterization to formally derive conformation space diffusion equations from kinetic theory. They proceed by applying the equivalent stochastic differential equations as a base for Brownian dynamics algorithm for chains with and without holonomic constraints. The vector parameterization framework allows the design of new parameterizations at will, i.e. in order to satisfy algorithmic requirements.

3.2. Cartesian rotation vector

The Cartesian components of the rotation vector are a set of generalized coordinates describing angular orientation and are given by [4]

$$\vec{a}(t) = \Phi(t) \vec{\delta}^{(a)}(\theta^{(a)}, \phi^{(a)}, t) := \{a_1(t), a_2(t), a_3(t)\}, \quad (20)$$

where the direction of the unit vector $\vec{\delta}^{(a)}$ is specified by the polar angles $\theta^{(a)}$ and $\phi^{(a)}$. The angle Φ describes the rotation about $\vec{\delta}^{(a)}$. The components of \vec{a} in the Cartesian space are defined in terms of the polar representation of the rotation vector

$$a_1 := \Phi \sin \theta^{(a)} \cos \phi^{(a)} \quad (21)$$

$$a_2 := \Phi \sin \theta^{(a)} \sin \phi^{(a)} \quad (22)$$

$$a_3 := \Phi \cos \theta^{(a)}. \quad (23)$$

For short, we call \vec{a} the Cartesian rotation vector. Note that $\Phi^2 = a_1^2 + a_2^2 + a_3^2$. From the definition in Eq. (20), it can be seen that $\vec{a} = (\Phi + 2\pi n) \vec{\delta}^{(a)}$ for all integer values of n . This means that the information associated with each of the following subspaces in the conformation space $\Phi \in [0, 2\pi), [2\pi, 4\pi), [4\pi, 6\pi), \dots$ is identical. These subspaces form spherical concentric shells, one outside the other. Naess and Elgsaeter [5] show that due to the symmetry $\vec{a} = (2\pi - \Phi) \vec{\delta}^{(a)} = -\Phi \vec{\delta}^{(a)}$, all possible angular orientations of the body are also included in the subspace

$$\Phi \in [0, \pi), \quad \theta^{(a)} \in [0, \pi], \quad \phi^{(a)} \in [0, 2\pi). \quad (24)$$

The Cartesian components of the rotation vector have not been employed previously in formal studies of rigid particle kinetic theory. Naess and Elgsaeter [4] use the choice $p(\Phi) = \Phi$ and provide the necessary mathematical expressions for transformations from \vec{a} to the Eulerian angles, and vice versa. In their preliminary efforts leading up to the latter work, the authors also found that there exists a choice for $p(\Phi)$, which yields a homogeneous equilibrium density in the rotation vector conformation space. This choice appeared not to offer any additional numeric benefits, and was therefore abandoned. They also present a diagram which shows how to determine ϕ , θ , and ψ when \vec{a} is given. In our work, we find the additional graphical approach in Fig. 3 to be very helpful. Using this figure, it is quite simple to gain a qualitative impression for how changes in the Eulerian angles affect \vec{a} . The vectors from the origin to a point in the rigid body before and after the rotation are denoted \vec{r} and \vec{r}' , respectively. For any value of ψ , the rotation vector is located in the plane that passes through the origin and is orthogonal to the plane defined by \vec{r} and \vec{r}' . The angles between this plane and the vectors \vec{r} and \vec{r}' are equal. The exact location of \vec{a} in this plane varies when ψ

is changed. For $\psi = 0$, the position of \vec{a} in this plane depends on the value of ϕ .

We end this section by illustrating how a plane with constant coordinate value transforms between Eulerian angles and

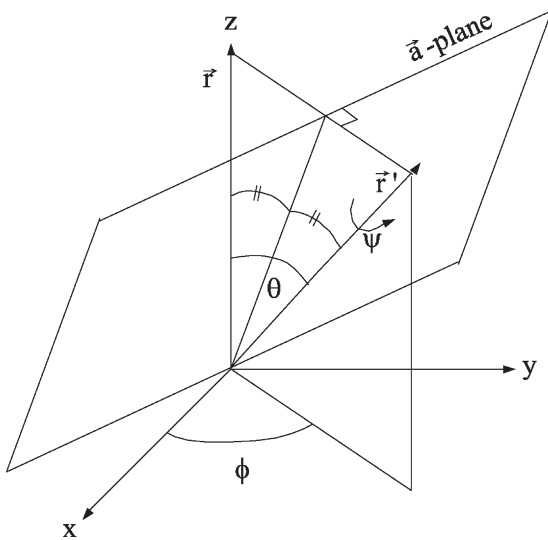


Fig. 3. Schematic illustration of how to determine the rotation vector for a given set of Eulerian angles. The vectors from the origin to a point in the rigid body before and after the rotation are denoted \vec{r} and \vec{r}' , respectively. The orientation in Eulerian angles are (ϕ, θ, ψ) . For any value of ψ , the rotation vector \vec{a} is located in the \vec{a} -plane, which passes through the origin, and is orthogonal to the plane determined by the vectors \vec{r} and \vec{r}' . The angles between the \vec{a} -plane and the vectors \vec{r} and \vec{r}' are identical. The exact position of \vec{a} varies when ψ is changed. For $\psi = 0$, the position of \vec{a} is a function of ϕ .

Cartesian rotation vector. Fig. 4 shows the plane $\psi = 0$ in various coordinate systems. Using Cartesian coordinates, this plane is the familiar sphere with the singularities at the poles. Transformation to Cartesian rotation vector, however, yields a non-singular surface in \vec{a} -space. The surface is formed as a ridge that runs along the negative a_1 -axis. Rotational diffusion in Eulerian polar coordinates (ϕ, θ) transforms into diffusion on this ridge.

3.3. Analytical expressions

After this compact introduction to the Cartesian rotation vector, we now compare some of the mathematical expressions presented in the previous section for the Eulerian angles with their Cartesian rotation vector counterparts. To obtain an expression for the potential energy of the dipole described earlier, we may apply Eq. (23) and a relation given in ref. [4]

$$\cos \theta = 1 - (1 - \cos \Phi) \sin^2 \theta^{(a)}. \quad (25)$$

Then, the potential energy reads

$$V(\vec{a}) = -\mu E \left\{ 1 - (1 - \cos |\vec{a}|) \left(1 - \frac{a_3^2}{|\vec{a}|^2} \right) \right\} - \frac{\nu \hat{\alpha}_1}{2} \left\{ 1 - (1 - \cos |\vec{a}|) \left(1 - \frac{a_3^2}{|\vec{a}|^2} \right) \right\}^2 - \frac{\nu \hat{\alpha}_2}{2} \left[1 - \left\{ 1 - (1 - \cos |\vec{a}|) \left(1 - \frac{a_3^2}{|\vec{a}|^2} \right) \right\}^2 \right] E_2. \quad (26)$$

This expression is more complex than its Eulerian angle counterpart, because all three Cartesian components of the rotation vector are needed. The expression describing the total birefringence is even more complex and will not be given here. However, using Eq. (25) and other similar expressions given by Naess and Elgsaeter [4], numerical values can easily be obtained and they are all without singularities for $|\vec{a}| \in [0, \pi)$. These singularity-free expressions are the main advantages of the Cartesian rotation vector components.

If we consider a spherical rigid body with no external forces acting on it, and we assume that the equilibrium probability density in conformation space is separable, $p(\vec{a}, t) = \Psi(\vec{a})f(t)$, the conformation space diffusion (Fokker–Planck) equation in Cartesian components of the rotation vector reads

$$\frac{\partial^2 \Psi}{\partial \vec{a}^2} - \frac{\partial}{\partial \vec{a}} \left[\left(\frac{\sin |\vec{a}|}{1 - \cos |\vec{a}|} - \frac{2}{|\vec{a}|} \right) \frac{\vec{a}}{|\vec{a}|} \Psi \right] = \frac{\lambda}{k_B T \mu_0} \Psi, \quad (27)$$

where μ_0 is the diagonal element of the rotational part of the mobility tensor, and λ is a time constant derived from $\partial f / \partial t = \lambda f$. Eq. (27) is non-singular in the subspace given by $|\vec{a}| \in [0, \pi)$.

3.4. Brownian dynamics analysis

The Cartesian components of the rotation vector in the subspace given by $|\vec{a}| \in [0, \pi)$, do not have the singularity difficulties associated with the Eulerian angles, and therefore may be the preferred choice for numerical simulations. Following the same procedure as for Eulerian angles, Naess and Elgsaeter [4] show that the expression for the metric force using Cartesian

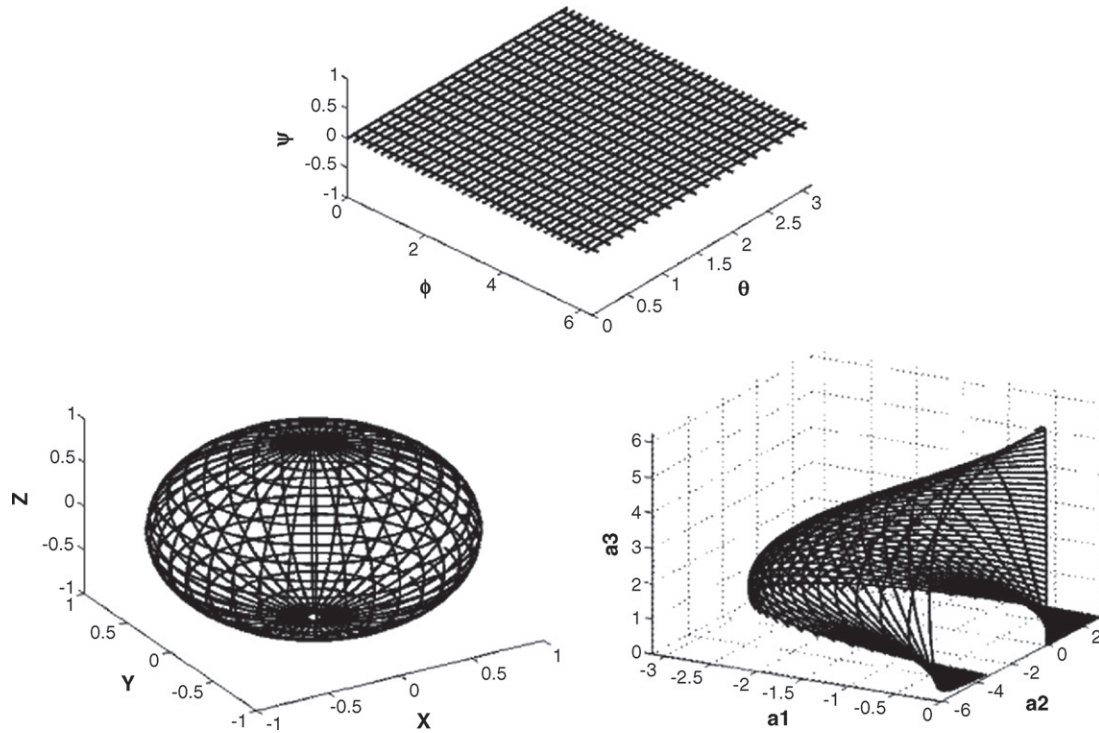


Fig. 4. (Top) Eulerian angles. The surfaces with constant ψ are planes parallel to the plane defined by the ϕ - and θ -axes. The shown plane corresponds to constant ψ ($\psi = 0$), and $\phi \in [0, 2\pi)$ and $\theta \in [0, \pi)$. (Bottom left) The surface that corresponds to constant ψ using polar coordinates in a regular Cartesian coordinate system. (Bottom right) The same surface transformed into Cartesian rotation vector space.

components of the rotation vector is given by

$$\vec{F}^{(m,rot)} = k_B T \left[\frac{\sin |\vec{a}|}{1 - \cos |\vec{a}|} - \frac{2}{|\vec{a}|} \right] \vec{\delta}^{(a)}. \quad (28)$$

Using power series expansions, it may easily be verified that Eq. (28) shows no singularity for $|\vec{a}| = 0$. In fact, the metric force equals $\vec{0}$ for $\vec{a} = \vec{0}$. The metric force is singular for $|\vec{a}| = \Phi = 2n\pi$, for integer $n \geq 1$. However, the fortunate finding that the numerical simulation can be limited to the part of conformation space given by $|\vec{a}| \in [0, \pi)$ facilitates avoiding this problem.

Naess and Elgsaeter [5] also demonstrate that the mobility tensor $\vec{\mu}^{*(a)}$ in Cartesian rotation vector conformation space shows no singularities.

3.5. Generalized force

Expressed in terms of the Cartesian rotation vector components, the rotational mobility tensor, $\vec{\mu}^{(a)}$, is defined by

$$\dot{\vec{a}} := \vec{\mu}^{(a)} \vec{F}^{(a)}, \quad (29)$$

where $\vec{F}^{(a)}$ is the generalized force associated with the Cartesian rotation vector components of the body in question. For a rigid body of ellipsoidal symmetry rotating with angular velocity $\vec{\omega}$ about its axis of rotational symmetry and the unit vector of $\vec{\omega}$ being time independent, the kinetic energy reads

$$\mathcal{K} = \frac{1}{2} I_1 \vec{\omega}^2 = \frac{1}{2} I_1 \dot{\Phi}^2. \quad (30)$$

Here, I_1 equals the principal value of the moment of inertia about the axis of rotational symmetry. When the axis of rotation coincides with the a_1 -axis, the angle of rotation equals a_1 , and the expression for \mathcal{K} becomes

$$\mathcal{K} = \frac{1}{2} I_1 \dot{a}_1^2. \quad (31)$$

For a potential $V(a_1) = -\mathcal{T}_1 a_1$, where \mathcal{T}_1 is the torque and a_1 is the angle of rotation, the conjugated generalized force reads

$$F_1^{(a)} = \frac{\partial}{\partial a_1} (\mathcal{K} - V) = -\frac{\partial V(a_1)}{\partial a_1} = -\frac{\partial (-\mathcal{T}_1 a_1)}{\partial a_1} = \mathcal{T}_1. \quad (32)$$

This means, in this special case, that the conjugated generalized force of a_1 simply equals the torque about the a_1 -axis. Similar results are obtained for rigid body rotation about the a_2 - or the a_3 -axis. This suggests that there are only three scalars that determine the rotational mobility of a rigid body. In turn, this suggests that in analysis of experimental data, e.g. transient birefringence of rigid bodies, it is not possible to determine more than three independent parameters.

4. Conclusion

This text compares the use of the Eulerian angles and the Cartesian rotation vector components as the generalized coordinates employed to describe the angular orientation of a rigid body in kinetic theory and Brownian dynamics analysis of molecular electro-optics. In most cases, the Eulerian angles yield relatively simple, yet singular, analytical expressions. The use of Cartesian rotation vector components, on the other hand,

result in non-singular behavior, but the analytical expressions tend to be more complex.

In a special case, we show that the generalized force associated with the Cartesian rotation vector equals the torque. In addition, we introduce a new graphical approach to qualitatively track how changes in the Eulerian angles affect the Cartesian rotation vector.

The absence of singularities in the numerical algorithms when the Cartesian rotation vector components are used as the generalized coordinates represents a major advantage. This makes the Cartesian rotation vector the most promising choice of generalized coordinates in numerical analysis of molecular electro-optics. Implementation and testing of algorithms for this purpose are in progress, and the results will be published at a later date.

Acknowledgement

This work was in part supported by Grant 158541/431 from the *Norwegian Research Council*.

References

- [1] R.P. Paul, Robot Manipulators, The MIT Press, Cambridge, 1981.
- [2] O.A. Bauchau, L. Trainelli, *Nonlinear Dynam.* 32 (2003) 71.
- [3] M.D. Shuster, *J. Astronaut. Sci.* 41 (1993) 439.
- [4] S.N. Naess, A. Elgsaeter, *Macromol. Theor. Simul.* 13 (2004) 419.
- [5] S.N. Naess, A. Elgsaeter, *Macromol. Theor. Simul.* 14 (2005) 300.
- [6] E. Fredericq, C. Houssier, *Electric Dichroism and Electric Birefringence*, Clarendon Press, Oxford, 1973.
- [7] A. Bjørkøy, A. Elgsaeter, A. Mikkelsen, *Biophys. Chem.* 72 (1998) 247.
- [8] S. Kim, S.J. Karilla, *Microhydrodynamics*, Butterworth-Heinemann, Boston, 1991.
- [9] S.N. Naess, A. Elgsaeter, *Macromol. Theor. Simul.* 11 (2002) 913.
- [10] R.B. Bird, C.F. Curtiss, R.C. Armstrong, O. Hassager, *Dynamics of Polymeric Liquids, Kinetic Theory*, vol. 2, second ed., Wiley, New York, 1987.
- [11] A. Mikkelsen, K.D. Knudsen, A. Elgsaeter, *Physica A* 66 (1998) 253.
- [12] S.N. Naess, H.M. Adland, A. Mikkelsen, A. Elgsaeter, *Physica A* 323 (2001) 294.
- [13] H. Goldstein, *Classical Mechanics*, second ed., Addison-Wesley, Reading, MA, 1980.
- [14] G. Strang, *Linear Algebra and its Applications*, third ed., Harcourt Brace & Company, Orlando, FL, 1988 (Chapter 4).

Paper II

Is not included due to copyright

Paper III

Is not included due to copyright

Paper IV

Is not included due to copyright

